British Geological Survey

Environmental monitoring in the Fylde, Lancashire - Phase 6 Final Report

Environmental Change and Adaptation Programme

Open Report OR/22/007

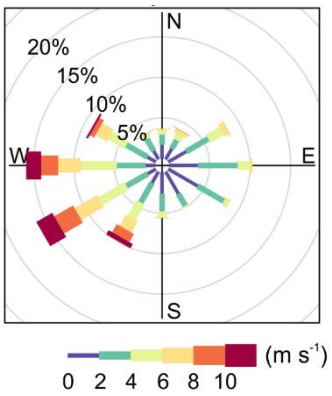

BRITISH GEOLOGICAL SURVEY

ENVIRONMENTAL CHANGE AND ADAPTATION PROGRAMME

OPEN REPORT OR/22/007

Environmental monitoring in the Fylde, Lancashire - Phase 6 Final Report

P. L. Smedley[1], J. T. Shaw[2], G. Allen[2] and E. Crewdson[1]

[1]British Geological Survey

[2]University of Manchester

Keywords

Atmospheric composition, groundwater, shale gas, hydrocarbons

Front cover

Preston New Road GHG monitoring site, wind rose showing direction, Fylde surface water. Windrose and air monitoring image © University of Manchester

Bibliographical reference

SMEDLEY, P.L., SHAW, J.T., ALLEN, G. AND CREWDSON, E. 2022. Environmental monitoring in the Fylde, Lancashire - Phase 6 Final Report. *British Geological Survey Open Report*, OR/22/007. 53 pp.

Keyworth, Nottingham British Geological Survey 2022

BRITISH GEOLOGICAL SURVEY

The full range of our publications is available from BGS shops at Nottingham, Edinburgh, London and Cardiff (Welsh publications only) see contact details below or shop online at www.geologyshop.com

The London Information Office also maintains a reference collection of BGS publications, including maps, for consultation.

We publish an annual catalogue of our maps and other publications; this catalogue is available online or from any of the BGS shops.

The British Geological Survey carries out the geological survey of Great Britain and Northern Ireland (the latter as an agency service for the government of Northern Ireland), and of the surrounding continental shelf, as well as basic research projects. It also undertakes programmes of technical aid in geology in developing countries.

The British Geological Survey is a component body of UK Research and Innovation.

British Geological Survey offices

Environmental Science Centre, Keyworth, Nottingham NG12 5GG

Tel 0115 936 3100

BGS Central Enquiries Desk

Tel 0115 936 3143
email enquiries@bgs.ac.uk

BGS Sales

Tel 0115 936 3241
email sales@bgs.ac.uk

The Lyell Centre, Research Avenue South, Edinburgh EH14 4AP

Tel 0131 667 1000
email scotsales@bgs.ac.uk

Natural History Museum, Cromwell Road, London SW7 5BD

Tel 020 7589 4090
Tel 020 7942 5344/45
email bgslondon@bgs.ac.uk

Cardiff University, Main Building, Park Place, Cardiff CF10 3AT

Tel 029 2167 4280

Maclean Building, Crowmarsh Gifford, Wallingford OX10 8BB

Tel 01491 838800

Geological Survey of Northern Ireland, Department of Enterprise, Trade & Investment, Dundonald House, Upper Newtownards Road, Ballymiscaw, Belfast, BT4 3SB

Tel 01232 666595
www.bgs.ac.uk/gsni/

Natural Environment Research Council, Polaris House, North Star Avenue, Swindon SN2 1EU

Tel 01793 411500 Fax 01793 411501
www.nerc.ac.uk

UK Research and Innovation, Polaris House, Swindon SN2 1FL

Tel 01793 444000
www.ukri.org

Website www.bgs.ac.uk
Shop online at www.geologyshop.com

Foreword

This report presents the results from Phase 6 of an independent environmental monitoring programme that was set up to investigate and monitor the environmental impacts of shale-gas exploration in England. The report is restricted to monitoring activities around the Preston New Road site in Lancashire and to monitoring of greenhouse-gas composition and water quality. This is due to the cessation of shale-gas exploration activities at the site following the imposition by the UK Government of the moratorium on high-volume hydraulic fracturing in England in November 2019. The report should be read in conjunction with previous reports on environmental monitoring in Lancashire and North Yorkshire that are available through the BGS project website (www.bgs.ac.uk/lancashire and www.bgs.ac.uk/valeofpickering). These provide additional background to the wider project and presentation of earlier results (2015–2019).

Acknowledgements

We especially thank Dan Mallin Martin, Alex Moir and Mike Bowes (BGS) for fieldwork assistance, laboratory radon analysis and calibration and maintenance of real-time sensor and telemetry equipment. BGS laboratory staff are acknowledged for chemical analysis of water samples. We also thank Mengyi Gong, formerly of BGS, for development of the R Shiny app for groundwater and Kathryn Leeming (BGS) for running it for the completed dataset. As ever, we are grateful to all landowners who have made sampling possible.

Contents

FIGURES

TABLES

Summary

This report concludes the period of independent environmental monitoring set up in the context of shale-gas exploration activities around the Cuadrilla Resources' Preston New Road (PNR) site in the Fylde, Lancashire. The report includes monitoring of greenhouse gases (GHGs) at the PNR site and monitoring of groundwater and surface-water quality around the site and more widely across the Fylde.

The report relates to monitoring in the years 2020–2022 (monitoring periods: February 2020 to January 2021 for GHGs, April 2020 to January 2022 for water quality). Cuadrilla's aborted hydraulic fracturing of the PNR site was conducted in 2018 and 2019 and so all monitoring detailed in this report relates to post-baseline. Cuadrilla surrendered the licences to carry out hydraulic fracturing at PNR in early 2020 following the UK Government's imposition of the moratorium on high-volume hydraulic fracturing in England in November 2019. Hence, it is believed that no further development took place at the site during the reporting period.

Atmospheric data for the PNR site showed that the dominant wind direction continued to be from the west, especially for the highest wind speeds (>4 m/s). Atmospheric CH_4 concentration data showed a background mixing ratio of around 1.90 ppm (equivalent to the northern hemispheric background CH_4), overlaid by short-term spikes of up to several ppm. The highest CH_4 mixing ratios were generally observed during periods of easterly winds, and were likely a result of emissions from a local dairy farm some 200 m east of PNR and longer-range urban and industrial pollution sources from the south-east. This is consistent with conclusions drawn for earlier phases of monitoring. Atmospheric CO_2 data showed distinct seasonal variation, with a decrease in background CO_2 mixing ratios during summer as a result of northern hemisphere biospheric respiration, also consistent with previous observations. As with CH_4, the highest CO_2 mixing ratios were observed during periods with easterly winds.

An algorithm for detection of CH_4 emissions related to operational activity, developed in previous phases of the monitoring, indicated three one-hour periods in March and May 2020 which exceeded threshold criteria. These were associated with exceptionally low wind speed (<1 m/s) and are considered unlikely to be due to actual fugitive emissions from PNR. A machine-learning method for detection of CH_4 fugitive emissions has also been developed using two different software tools. The tool using each was able to forecast the timing and location of transient spikes in CH_4 mixing ratios, although the models often failed to forecast the exact magnitude of above-background enhancement. The machine-learning tool will be developed further and reported elsewhere.

Monitoring data for GHGs over the whole monitoring programme (5 years) have shown a gradual increase in the observed background mixing ratios of both CH_4 and CO_2, consistent with increases in northern hemispheric background concentrations. Monitoring data suggest a gradual increase in northern hemispheric background CH_4 mixing ratios of several ppb per year.

Four rounds of monitoring were carried out for water quality during the project period. These mostly focused on groundwater and on locations from the Quaternary aquifer relatively close to PNR. As with previous monitoring, considerable spatial variability in inorganic chemical composition is evident. Temporal variability is also considerable for the few monitored streams. Temporal variation appears less for the monitored groundwaters, though one site showed statistically significant differences in concentration for some analytes after October 2019 when compared with before. However, this difference is not believed to be due to PNR activity.

Statistical modelling of monitoring data for groundwater inorganic chemical compositions in the Quaternary aquifer has attempted to account for the observed spatial and temporal variation under baseline conditions and compare with post-baseline compositions for each round of

subsequent monitoring. In the post-baseline period, a number of individual sites showed concentrations for a number of analytes outside the 95% confidence intervals for the expected standardised mean values. Exceedances occurred most frequently for specific electrical conductance. Values outside the confidence intervals were not consistent between analytes or across sites and recording of a number of false positives is likely, reflecting the uncertainties caused by the large space-time heterogeneity in groundwater compositions. No sites showed consistent exceedances for dissolved CH_4, one of the key analytes monitored for evidence of potential leakage from sub-surface hydrocarbon sources. For data modelled from the Preston New Road site only, fewer values occurred outwith the 95% confidence intervals for the standardised mean, likely reflecting the reduced heterogeneity at site compared to regional scale.

Data for a suite of organic chemicals in the rounds of sampling for 2020–2021 showed concentrations overwhelmingly below analytical detection limits and therefore did not reveal evidence for contamination from previous hydraulic fracturing activities.

Likewise, real-time data from groundwater sites monitored across the Fylde for specific electrical conductance, of value as a potential indicator of influx of deep saline fluids from hydraulic fracturing activities, has not shown evidence for increased salinity over time.

By continuing to monitor GHGs and water quality under baseline conditions and following Cuadrilla's hydraulic fracturing activities at PNR, detailed data and evidence has been provided to establish the spatial and temporal variabilities and to explore statistical approaches to establishing deviations from baseline. Such investigations are needed to monitor the risks from deep exploration activities and to provide public confidence in areas of environmental concern. The approaches used have application in broader areas of environmental monitoring, including of sub-surface industrial developments other than unconventional hydrocarbons.

1 Introduction

Independent environmental monitoring activities in the context of English shale-gas exploration have been carried out by BGS in collaboration with university and Public Health England partners at the proposed and actual exploration sites in the Fylde, Lancashire and the Vale of Pickering, North Yorkshire. The monitoring has been carried out in five previous phases since 2015. This report describes activities and findings from Phase 6, the final period of the environmental monitoring programme. As a result of the imposition of the moratorium on high-volume hydraulic fracturing in England and the cessation of plans to carry out high-volume hydraulic fracturing at Third Energy's site at Kirby Misperton in the Vale of Pickering, the Phase 6 reporting relates solely to monitoring activities carried out in the Fylde, where hydraulic fracturing has taken place.

The activities reported in Phase 6 (2020–2022) are also restricted to monitoring of GHGs and water quality as these were deemed to be the environmental compartments more likely to carry risks from post-hydraulic-fracturing activities. Seismicity, a major component of previous phases of the programme, was not pursued in the absence of further hydraulic fracturing after 2019 as the seismic risk was considered now to be very low. Seismometers installed around PNR in the earlier phases of monitoring were removed after 2019 but seismicity monitoring in the region more widely continues as part of the UKArray.

The original planned timetable for Phase 6 was April 2020 to March 2021. The actual timetable was disrupted significantly and extended by 10 months as a result of the mitigation required for the logistical impacts of Covid-19. Public-engagement activities have necessarily been minimised as a result of both lack of activity at PNR following the moratorium and Covid-19 restrictions. The BGS websites have been maintained, ad-hoc enquiries handled and landowner discussions in relation to site visits conducted, but other public interactions have not been appropriate.

2 Atmospheric greenhouse gases

2.1 BACKGROUND

This report discusses measurements of GHGs sampled near the PNR monitoring station during the Phase 6 period: 1st February 2020 – 31st January 2021. The previous four years of continuous monitoring, consistent with Phases 2 through 5 of the Environmental Baseline Project, were reported on in earlier work (Ward et al., 2017; Ward et al., 2018b; Ward et al., 2019; Ward et al., 2020). It is assumed that the reader is familiar with these reports and the reader is directed to them for further detail regarding instrumentation and sampling, as well as prior conclusions regarding these earlier phases of work. Briefly, and in the context of GHGs, Phases II and III (1st February 2016 – 31st January 2018), during which time the hydraulic fracturing facility was constructed, were used to establish a baseline of local methane and CO_2 mixing ratios, along with meteorological conditions. Exploratory hydraulic fracturing for shale gas then began in Phase 4 and continued in Phase 5 (1st February 2018 – 31st January 2020), with the fracturing of, and flow-testing from, two wells: PNR 1Z and PNR 2.

The fifth year of measurements (Phase 6; February 2020 to January 2021) was severely impacted by the Covid-19 pandemic. The UK Government advised limiting non-essential travel on 16th March 2020, before placing the country into a national lockdown on 23rd March 2020. Whilst phased reopening began towards the end of June 2020, some localised restrictions on travel continued throughout the summer. Rising Covid-19 cases towards the end of summer prompted the UK Government to reinstate some national restrictions across England in September 2020, followed by a three-tier system in October 2020. A second national lockdown

began on 5th November 2020, ending on 2nd December 2020, but with many localised restrictions kept in place, especially throughout much of north-west England. A fourth tier of restrictions was first introduced on 21st December 2020, with much of England placed into Tier 4 on 26th December 2020. England then entered a third national lockdown on 6th January 2021.

The implementation of the three nationwide lockdowns, as well as the intervening localised restrictions, had several major consequences for atmospheric composition monitoring throughout Phase 6. Firstly, regular site visits were not possible to conduct, preventing the frequent instrument calibration regime necessary for high-quality data. Site maintenance was also not possible, resulting in two periods of complete loss of power to the monitoring station, thought to be a result of adverse weather conditions. The two periods were: 6th August 2020 – 25th August 2020 and 10th September 2020 – 31st January 2021 (this power outage continued until the monitoring site was decommissioned on 3rd June 2022). These outages resulted in a loss of approximately 44% of data within Phase 6.

No industrial activity at the PNR site is thought to have occurred during Phase 6 as a result of the moratorium on hydraulic fracturing imposed by the UK Government on 2nd November 2019. Measurements of GHGs were continued in order to monitor the legacy of wells on the Cuadrilla-owned shale-gas-extraction facility for leaks of CH_4 and/or CO_2. Unfortunately, information regarding the presence of any leak control arrangements, such as plugging or sealing of the fractured wells, is not known to be publicly available at the time of writing. Equally, the exact processes involved in decommission remain unknown.

2.1.1 Additional references

Several peer-reviewed journal articles discussing various aspects of the atmospheric monitoring relevant to this project have now been published (or are in preparation) in addition to the annual reports cited above. The reader is directed to these for additional and detailed scientific analysis.

1. Purvis et al. (2019) analysed baseline and pre-operational concentrations of NO_x and other air-quality (AQ) indicators at the Kirby Misperton (KM), Yorkshire, monitoring site.
2. Shaw et al. (2019) described a baseline of GHGs at both PNR and KM, prior to operational activity at either site. An algorithm for the identification of periods of elevated CH_4 mixing ratios statistically outside of the typical range of baseline mixing ratios was also presented.
3. Lowry et al. (2020) described the monitoring of shale-gas development using mobile measurement methods, and the identification and characterisation of other local CH_4 sources in the vicinity of PNR and KM.
4. Shaw et al. (2020) reported the detection of a period of significantly enhanced CH_4 mixing ratios, coincident with operator-reported emissions during flowback activities. Three independent flux quantification methods were used to derive a CH_4 emission flux for this event. An initial report of this event can also be found in a BGS web publication (Allen et al., 2019).
5. Shah et al. (2020a) reported the same event as Shaw et al. (2020) but used an unmanned aerial vehicle (UAV) for detection and quantification of CH_4 emissions during flowback. Shah et al. (2020b) presented an overview of the UAV-based method used for detection and quantification of CH_4 emissions.
6. Shaw et al. (*in prep.*) have used machine-learning tools to detect anomalous CH_4 mixing ratios associated with CH_4 emission events, as an alternative to the manually-derived statistical algorithm presented in Shaw et al. (2019).

2.2 MONITORING ACTIVITIES

The monitoring site at KM was decommissioned for both AQ and GHG measurements on 26th February 2020, as it was determined that no further shale-gas exploration was likely

following public statements made by the site operator (Third Energy). No data from KM will be presented in this report.

GHG data continued to be collected at the fixed-site monitoring station located at PNR during Phase 6, except for between 6th and 25th August and after 10th September 2020 due to localised power outages. The inaccessibility of the site during national lockdowns meant that site maintenance was impossible and the power outages prevailed. No AQ measurements at PNR were made during Phase 6 and this report discusses GHG measurements only. The monitoring station at PNR was decommissioned for both AQ and GHG measurements on 3rd June 2021.

2.2.1 Data calibration and quality assurance

The calibration and quality assurance procedures outlined in the Phase 2 report (Ward et al., 2017) have not been upheld during this Phase of monitoring, as a direct result of Covid-19. The final instrument calibration took place on 22nd January 2020. All data after that date used this final calibration point to calibrate the raw data. However, it is extremely likely that there was long-term instrumental drift in the operation of the GHG instrumentation that cannot be accounted for after 22nd January 2020. All data after this date should be considered to be of reduced quality. The data have been made available to view publicly on the Centre for Environmental Data Analysis (CEDA) archive (www.CEDA.ac.uk) but with the caveat of reduced data quality.

2.3 ANALYSIS AND DISCUSSION

The following sections describe the GHG measurements made during Phase 6 of the Environmental Monitoring Project. Readers are referred to the Phase 5 report (Ward et al., 2020) for analysis of the previous four years of GHG (and AQ) measurements.

As no instrument calibrations were able to take place during Phase 6 due to Covid-19, the data are of reduced quality relative to previous phases of work.

Table 1. Details of the 12-month atmospheric gas measurement periods

Period start	Period end	Year number	Reporting phase	Report reference
1st February 2016	31st January 2017	1	2	Ward et al. (2017)
1st February 2017	31st January 2018	2	3	Ward et al. (2018b)
1st February 2018	31st January 2019	3	4	Ward et al. (2019)
1st February 2019	31st January 2020	4	5	Ward et al. (2020)
1st February 2020	31st January 2021*	5	6	This work

* No measurements after 10th September 2020

2.3.1 PNR wind climatology

The wind field regime at PNR during Phase 6 was very similar to those measured during the previous phases of work (see Appendix 1). The dominant wind direction continued to be from the west, especially for the higher wind speeds (i.e. those greater than 4 m/s).

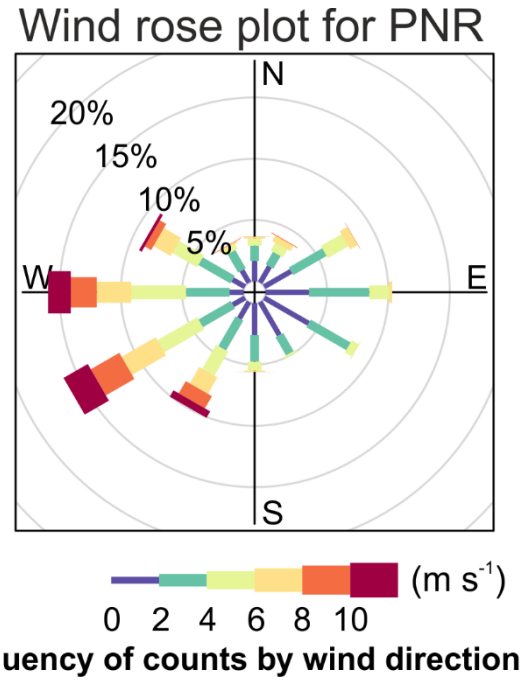

Figure 1. Wind-rose plot for the PNR site showing wind speed and wind direction statistics for Phase 6 (1st February 2020 – 31st January 2021*). The radii of the paddles show the percentage of total sampling time in each of the 12 30° wind direction cones. The colour and length of the sectors indicate the percentage of time in each wind-speed band (see colour legend)
*No data recorded after 10th September 2020 owing to power outage at the monitoring station

2.3.2 PNR greenhouse gases

Figure 2 shows a time series of one-hour averaged CH_4 mixing ratios measured at PNR during Phase 6. The data were broadly similar to previous phases of measurement (Appendix 1), with a background mixing ratio of roughly 1.90 ppm (equivalent to the northern hemispheric background CH_4), overlaid by short-term transient spikes in CH_4 of up to several ppm. The short-term spikes (generally less than three hours in duration) are thought to be associated with rapidly changing meteorological conditions, or easterly winds, which are accompanied by CH_4 emissions from a local dairy farm (ca. 200 m to the east of the monitoring station). The one-minute average values were also consistent with those measured during previous phases.

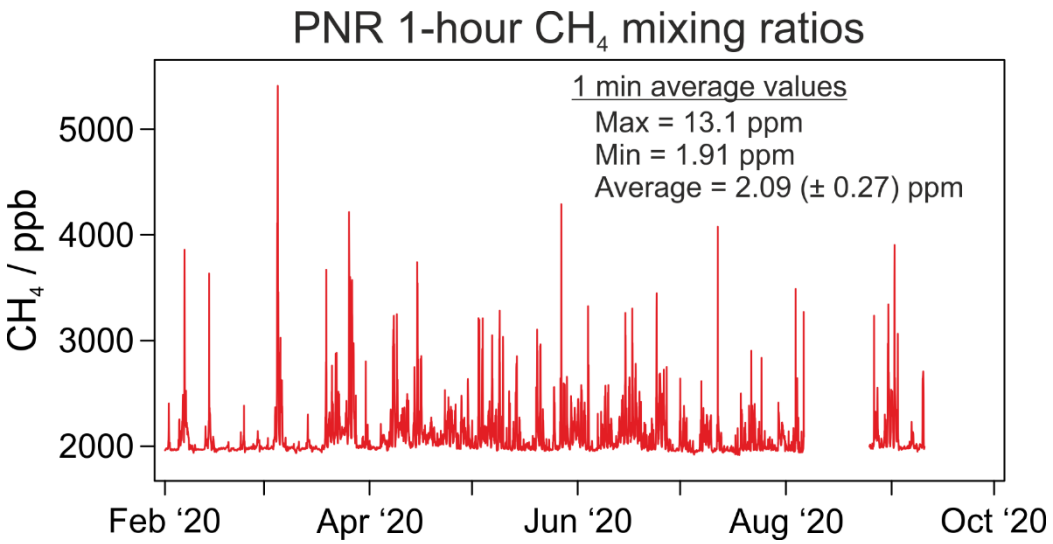

Figure 2. Time series of one-hour-averaged CH_4 mixing ratios measured at PNR during Phase 6 (1st February 2020 – 31st January 2021*)
*No data recorded after 10th September 2020 owing to power outage at the monitoring station

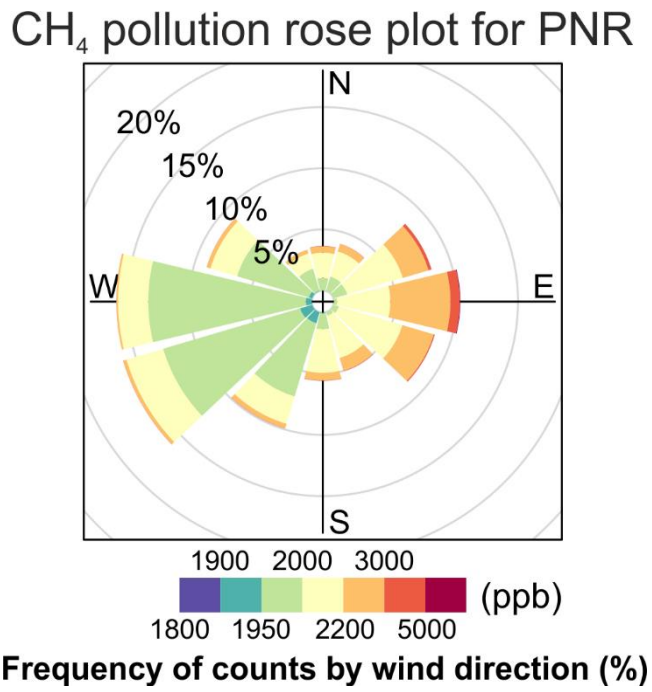

Figure 3. CH_4 concentration-frequency and wind-rose plots showing CH_4 mixing ratios as a function of wind direction during Phase 6 (1st February 2020 – 31st January 2021*). The radii of the paddles show the percentage of total time in each of the 12 wind direction cones (30° increments relative to true North) and the colour of the paddles shows the CH_4 mixing ratio (see colour legend).
*No data recorded after 10th September 2020 owing to power outage at the monitoring station

Figure 3 shows a pollution rose plot of CH_4 mixing ratios measured at PNR during Phase 6 (Appendix 1). The highest CH_4 mixing ratios were generally observed to occur during periods of easterly winds, and were likely a result of emissions from the local dairy farm to the east, and longer-range (longer temporal and more chemically and dynamically mixed) urban and industrial pollution sources to the south east (including cities such as Manchester, Birmingham, and London). CH_4 mixing ratios were generally lower under westerly wind conditions, consistent with

other phases of work. Westerly winds bring 'clean' air from over the Atlantic, free of many polluting sources, and can be considered to be broadly representative of the Northern Hemispheric methane background. However, the frequency of CH_4 mixing ratios below 1900 ppb has been decreasing steadily year-on-year, reflecting the gradual increase in northern hemispheric background CH_4 mixing ratios of several ppb per year (Section 2.3.4).

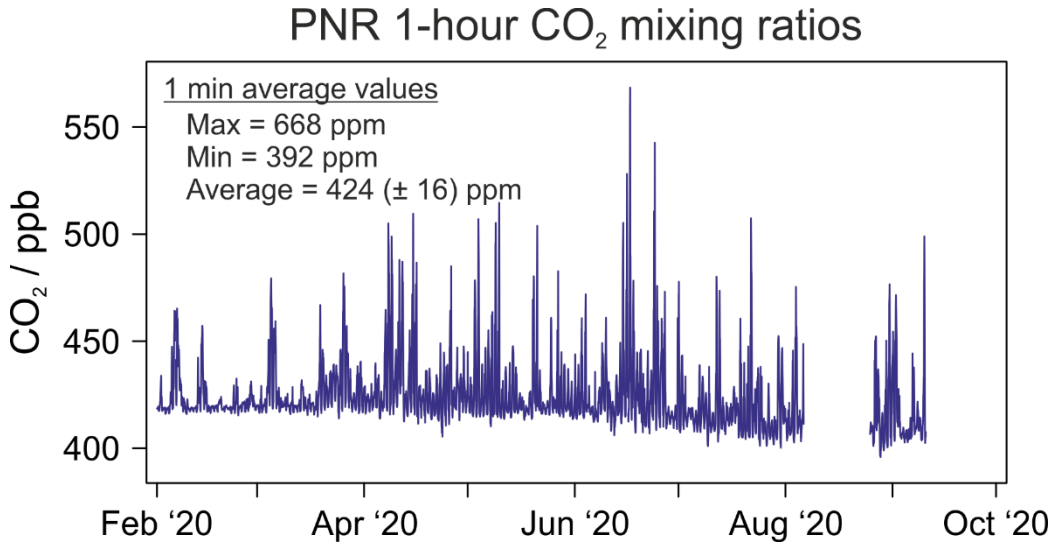

Figure 4. Time series of one-hour-averaged CO_2 mixing ratios measured at PNR during Phase 6 (1st February 2020 – 31st January 2021*)
*No data recorded after 10th September 2020 owing to power outage at the monitoring station

Figure 4 shows a time series of one-hour-averaged CO_2 mixing ratios measured at PNR during Phase 6. As for CH_4, the CO_2 data were similar to that measured during previous phases (Appendix 1). The seasonal variation was distinct, with a decrease in background CO_2 mixing ratios during summer months as a result of northern hemisphere biospheric respiration. One-minute average values were again consistent with previous data, despite the lack of measurements after 10th September 2020.

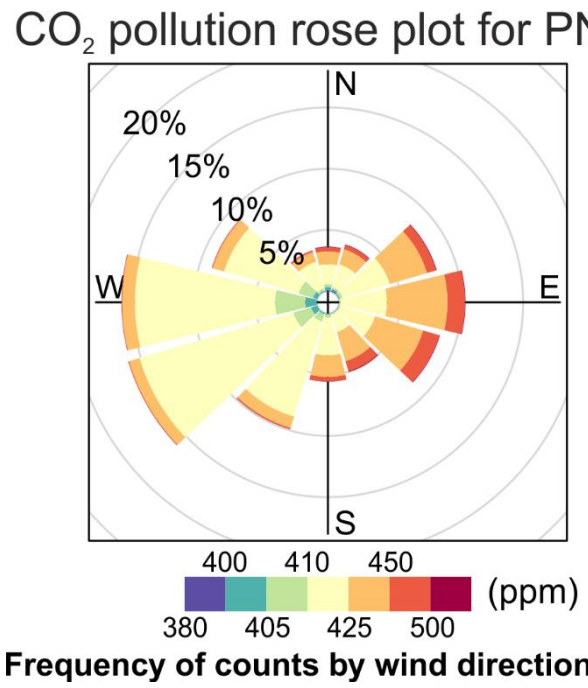

Figure 5. CO_2 concentration-frequency and wind-rose plots showing CO_2 mixing ratios as a function of wind direction during Phase 6 (1st February 2020 – 31st January 2021*). The radii of the paddles show the percentage of total time in each of the 12 wind direction cones (30° increments relative to true North) and the colour of the paddles shows the CO_2 mixing ratio (see colour legend)
*No data recorded after 10th September 2020 owing to power outage at the monitoring station

Figure 5 shows a pollution rose plot of CO_2 mixing ratios measured at PNR during Phase 6 (see also Appendix 1). The highest CO_2 mixing ratios were generally observed to occur during periods of easterly winds, and were likely a result of emissions from the local dairy farm to the east, and longer-range (longer temporal and more chemically and dynamically mixed) urban and industrial pollution sources to the south-east (including cities such as Manchester, Birmingham, and London). CO_2 mixing ratios were generally lower under westerly wind conditions, consistent with other phases of work. Westerly winds bring 'clean' air from over the Atlantic, which is free of many polluting sources. However, the frequency of CO_2 mixing ratios below 410 ppm has been decreasing steadily year-on-year, reflecting the gradual increase in northern hemispheric background CO_2 mixing ratios of several ppm per year. This is consistent with conclusions drawn for earlier phases.

2.3.3 Impact of industrial activities on measured greenhouse gases at PNR

Operational activity should not have taken place at the Cuadrilla-owned shale-gas facility at PNR during Phase 6, due to the moratorium placed on hydraulic fracturing by the UK Government in November 2019 and the subsequent closure of the site. However, the status of the two PNR wells that were drilled and hydraulically fractured is unknown at the time of writing. Fugitive emissions of CH_4 from abandoned, decommissioned, and even sealed wells are known to occur, and substantial methane leaks have been measured in many cases previously (e.g. Sandl et al., 2021; Williams et al., 2021; Riddick et al., 2020; Boothroyd et al., 2016). Hence, continued scrutiny of greenhouse-gas measurements at the PNR site is necessary, to determine if fugitive emissions are occurring.

The algorithm for detection of CH_4 emissions related to operational activity at PNR is presented in Appendix 2. The algorithm is based on threshold criteria for the identification of CH_4 mixing

ratios statistically outside of those measured during the baseline period (Phases 2 and 3) and is described in further detail by Shaw et al. (2019) and Ward et al. (2019).

Three one-hour periods exceeded the threshold criteria and were identified by the algorithm in Phase 6. These occurred at 08:00:00 19th March 2020, 22:00:00 11th May 2020, and 23:00:00 26th May 2020. All three of these periods were characterised by exceptionally low wind speeds (generally below 1 m/s but also often below the instrument limit of detection for wind speed measurement, equal to 0.3 m/s), and highly variable wind direction. The one-hour mean CH_4 mixing ratios during these three periods were 2689, 2521, and 2643 ppb for 19th March, 11th May, and 26th May 2020 respectively. As such, these three periods were unlikely to be associated with fugitive emissions from the shale-gas site, and were likely falsely identified by the threshold algorithm. This is consistent with conclusions from previous reports, in which the threshold algorithm identified a small fraction of hourly periods despite no reported emissions from the shale gas operator.

A second method tested for detecting and identifying anomalous CH_4 mixing ratios that could be associated with emissions from the shale-gas site involved the use of machine-learning. Machine-learning tools are able to process large amounts of data very quickly, and hence may find use for atmospheric monitoring and emission detection. Shaw et al. (*in prep*.) uses two different machine-learning tools (*rmweather* and Prophet) to quickly and efficiently identify periods of CH_4 emission during operator-reported flowback operations – the same periods identified using the manually-derived threshold algorithm used in Shaw et al. (2020). The use of machine-learning requires no prior expert knowledge of atmospheric emissions. This is not true of the threshold algorithm, which required extensive statistical analysis of GHGs and AQ pollutants over different time periods (days, weeks, months, seasons, years), as well as understanding of atmospheric transport and dispersion.

The two machine-learning tools work in different ways. Briefly, *rmweather* utilises a random forest (or decision forest) approach, and has been used previously to conduct meteorological normalisation on atmospheric composition data for trend analysis and for detecting the influence of air-quality interventions (e.g. Grange et al., 2018; Grange and Carslaw, 2019). *rmweather* has recently been used to forecast business-as-usual, or counterfactual, datasets, to assess the impacts of Covid-19 lockdowns on air quality (e.g. Grange et al., 2021; Lovric et al., 2021, Shi et al., 2021). Prophet is a time-series forecasting tool used to decompose temporal trends in data (Taylor and Letham, 2018). Prophet has been used to identify reductions in NO_2 concentrations in Manchester, UK, as a result of national lockdowns during the COVID-19 pandemic (Topping et al., 2020).

Both *rmweather* and Prophet can be used to forecast CH_4 mixing ratios using the relationship between CH_4 and co-measured variables (e.g. CO_2 mixing ratios, wind speed, wind direction, air temperature, atmospheric pressure, as well as different temporal indicators – hour-of-day, day-of-week, month, Julian date etc.). The two tools were trained for these relationships using baseline data (Phases 2 and 3) in the absence of the shale-gas extraction facility. Once trained, the tools were used to forecast (in the perspective of the machine-learning tools) CH_4 based on the measured values of the other variables in Phases 4, 5, and 6. The forecasts are unable to account for CH_4 emissions from the shale-gas extraction facility, and therefore represent a business-as-usual, or counterfactual, dataset to that actually measured. If the forecast methane differs considerably from the measured CH_4 mixing ratio, this would indicate a “new” methane emission source not present in the training baseline data.

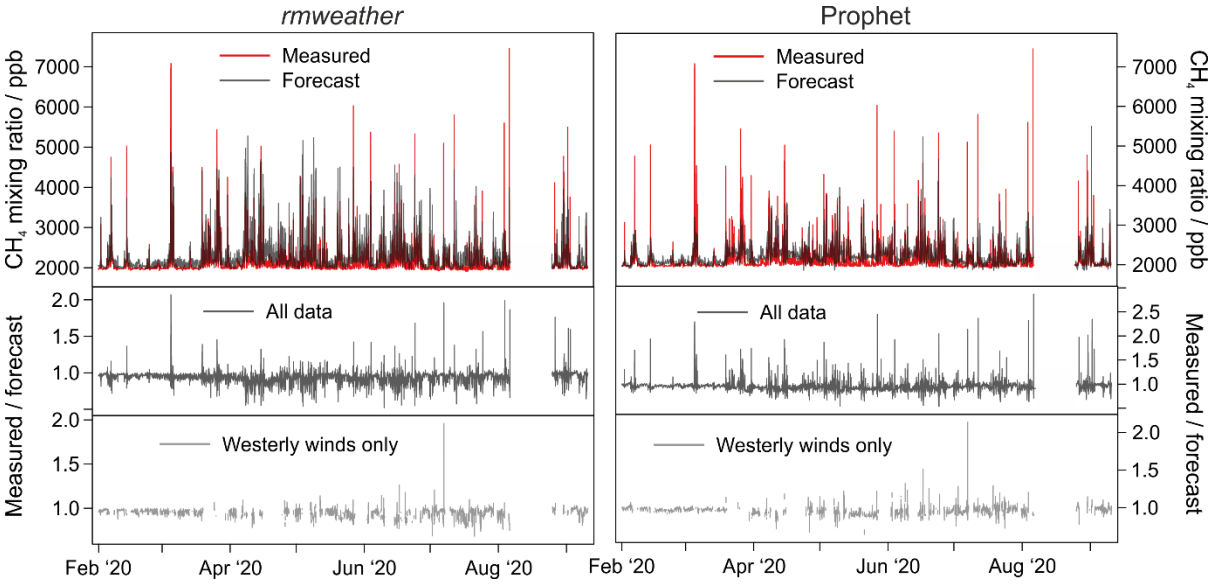

Figure 6. Comparison of measured and forecast CH_4 mixing ratios during Phase 6, using the *rmweather* package (left) and Prophet (right). The lower panels show the ratio of measured-to-forecast methane mole fraction, with the data in the bottom panels filtered to only show periods in which the wind direction was westerly (270° ± 45°)

Figure 6 shows the results of applying the two machine-learning tools to 10-minute average Phase 6 data. Forecast CH_4 mixing ratios were in broad agreement with those measured throughout the year, although both tools overestimated the background CH_4 during the summer months. The timing and location of the short-term transient spikes in CH_4 mixing ratios were generally captured by the forecasts, although the tools often failed to precisely capture/forecast the exact magnitude of enhancement above background. However, this does not impact the ability of the tool to isolate periods of clear interest in the context of unexpected emissions. Local methane mixing ratios are influenced by more than just the local meteorological conditions (i.e. the only variables that the machine-learning tools were trained on). Unusual circumstances both regionally and globally are also likely to have small influences on local methane mixing ratios. As an example, the global methane background experienced a much larger increase in 2020 than it had done in previous years and the machine-learning forecasts could not account for that (Lan et al., 2021; https://gml.noaa.gov/ccgg/trends_ch4/).

The lower panels in Figure 6 show the measured-to-forecast ratios, with the bottom panels filtered to only show periods in which the wind direction was westerly (270° ± 45°). Forecast CH_4 mixing ratios were generally within a factor of 2 of those measured, but were typically much closer to one during periods of westerly winds. Only one instance occurred where the measured-to-forecast ratio exceeded 1.5 (for both tools) during a period of westerly winds; on 7th July 2020 at 06:00:00. The wind speed at the time was exceptionally low (approximately 1 m/s) and the wind direction switched rapidly from southerly to westerly. Therefore, the high CH_4 mixing ratios at this time were unlikely to be the result of fugitive CH_4 emissions from the shale-gas site. For comparison, the measured-to-forecast ratios during known emission events were generally greater than 3 (Shaw et al., *in prep.*).

2.3.4 Long-term trend

Figure 7 shows the long-term trend in background CO_2 and CH_4 mixing ratios measured at PNR. The background was derived by filtering the entire dataset (ca. 5 years) for westerly wind conditions (270° ± 45°) and by removing data during stagnant wind conditions (< 3 m/s), before calculating monthly average mixing ratios for each of CO_2 and CH_4.

There has been a clear increase in the background CO_2 mixing ratio over the 4.5 years since measurements began. The seasonal cycle of CO_2 was pronounced in all years, although the decrease in CO_2 associated with biospheric uptake in summer 2020 took place slightly later relative to other years.

There has also been a gradual increase in the background CH_4 mixing ratio, consistent with increases in northern hemispheric background CH_4. The seasonal cycle of CH_4 was less clear than that for CO_2. A spike in background CH_4 mixing ratios occurred in August 2017, but its cause is unknown. No activity was thought to have been taking place at the shale-gas facility at the time.

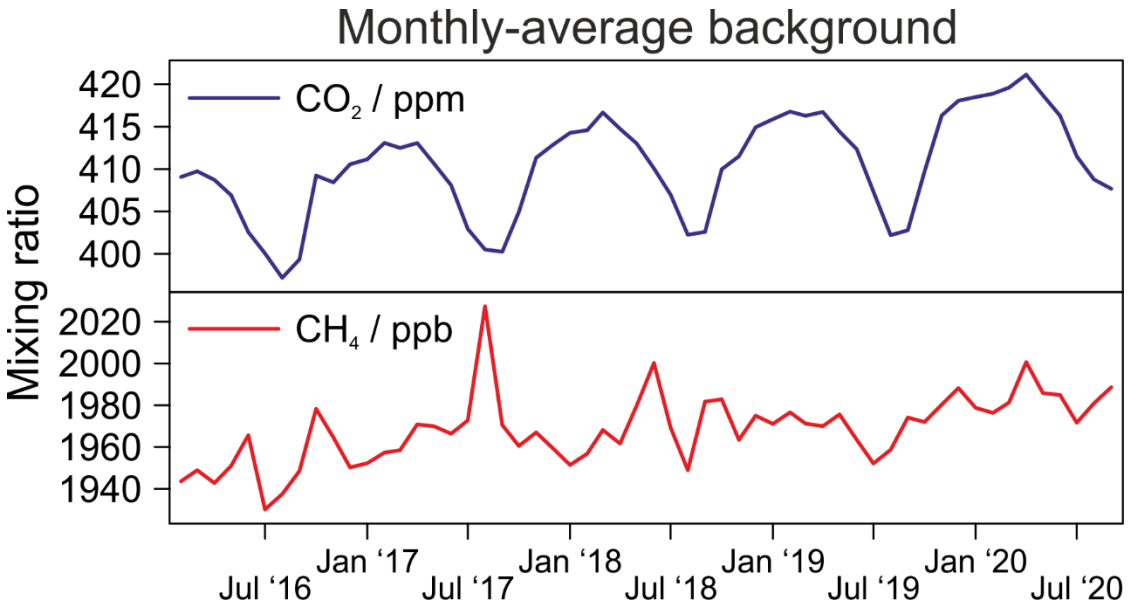

Figure 7. Monthly-average background CO_2 and CH_4 mixing ratios at PNR

3 Water-quality monitoring

3.1 MONITORING APPROACH AND SCHEDULE

Background to the hydrogeology and the water monitoring programme in the Fylde were detailed by Ward et al. (2018a) and previous monitoring data were described by Ward et al. (2020). Phase 6 water-monitoring investigations, including fieldwork planning, sampling, analysis and interpretation were conducted over the period April 2020 to January 2022. Original planning envisaged quarterly monitoring of selected sites in the established monitoring network (Figure 8) and writeup over the 12 months from April 2020. The extended period is due to pandemic-related delays and associated access restrictions.

Four water monitoring rounds were conducted over the period: August 2020, November 2020, July 2021 and October 2021. The monitoring focused on sites close to the PNR shale-gas site and boreholes from the Quaternary deposits as these were considered more likely to have been impacted by site activities than those at a greater lateral distance; borehole sites in the Sherwood Sandstone (east of the Woodsfold Fault; Figure 8) were therefore not sampled in this phase. Sampling also concentrated mainly on groundwater although a small number of streams close to PNR were sampled in the third and fourth rounds of sampling.

Efforts were made to sample the boreholes on the PNR well pad but this was not possible in the period as we were unable to gain permission from the operator as the site was not operational.

To compensate, the number of water samples collected was augmented from the cohort of sites accessible in the BGS and third-party-owned network.

As in previous project phases, sites were sampled on-site for unstable parameters (pH, temperature, dissolved oxygen, electrical conductance) and in the laboratory for major ions, a comprehensive suite of trace elements, dissolved gases (CH_4 and CO_2; groundwater only) and a suite of organic compounds. Laboratory analysis of inorganic solutes and organic compounds followed UKAS-accredited procedures at BGS and commercial laboratories.

Hydraulic fracturing took place in PNR boreholes 1Z and 2 over the periods October–December 2018 and August 2019 respectively. All the water sampling in the current phase is therefore considered as post-baseline.

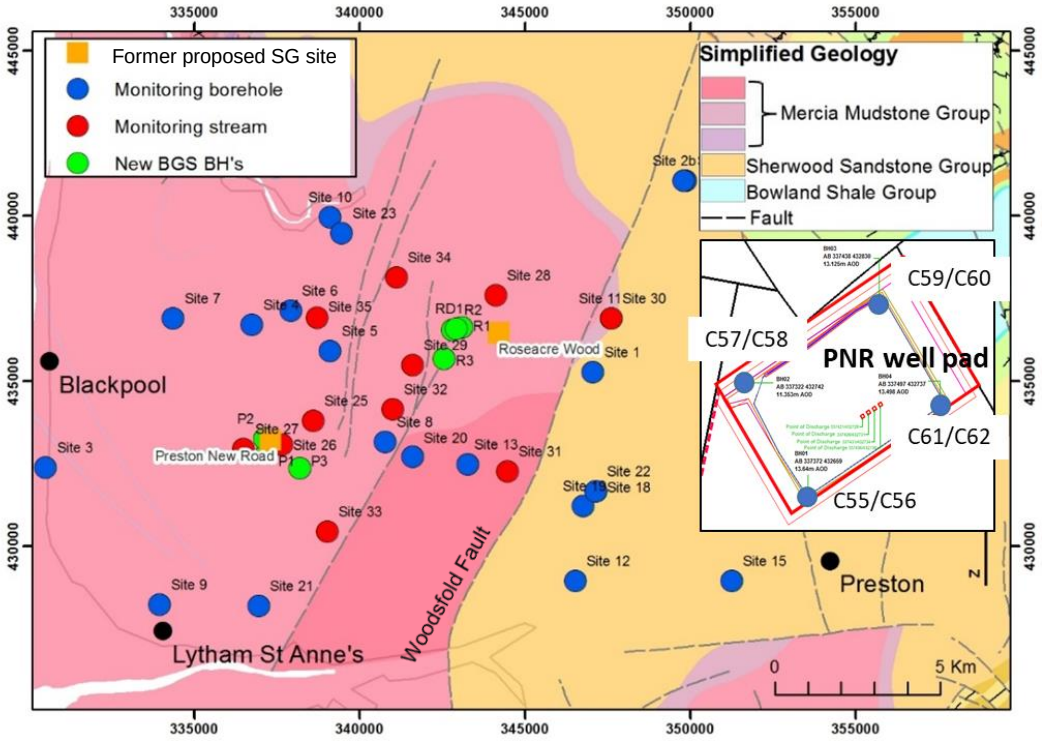

Figure 8. Simplified bedrock geological map showing the locations of water sampling sites in the Fylde water-monitoring network. Sites marked in green are BGS water-monitoring boreholes clustered around the Roseacre Wood (R) or Preston New Road (P). Inset shows water monitoring boreholes on the Preston New Road (PNR) well pad

3.2 MONITORING RESULTS

A substantial body of data has been amassed for water quality at monitored sites over the phases of the project. Plots showing monitoring data include results from the previous phases. Figure 9 shows the temporal variation in selected inorganic analytes from sites in the monitoring network within the shallow Superficial (Quaternary) aquifer. These include the major ions and a range of detectable trace elements. The samples are taken from third-party-owned boreholes. Results are shown for 2015 to 2021; intervals when hydraulic fracturing took place in boreholes PNR 1Z and 2 are also shown. The water-chemistry data show considerable temporal variability for some analytes, although no clear trends are visible from the plot.

Figure 10 shows the temporal variability for the same analytes for groundwater from the BGS-installed boreholes, also in the Superficial aquifer, for the period 2016 (when installed) to 2021. The more frequent monitoring over the hydraulic fracturing periods is evident, as is the similar temporal variability for many of the analytes. No temporal trends are clearly visible, with the exception of Site B44 (purple), which indicates slight increases in concentrations of Ca,

alkalinity, Cl, I and Mn (Figure 10) as well as in concentrations of Br, dissolved CO_2, rare earth elements and electrical conductance (not shown). These variations are accompanied by a slight but significant (at 95%) decrease over time in groundwater pH (6.97 ± 0.14 before October 2019 (arbitrary date), 6.63 ± 0.06 after, $p<<0.05$). The borehole is located at R3 (Figure 8). This is one of a cluster of boreholes sited around the Roseacre Wood former proposed hydraulic fracturing site. As the site is the only one with clear trends in concentrations of some analytes and as it is relatively remote from the site of actual hydraulic fracturing (PNR) compared to the PNR cluster ('P' sites), this is considered unlikely to be linked to the 2018–2019 hydraulic fracturing. Inferences on causes of the decreasing pH are speculative but might relate to changes at surface, including inputs of organic material. The borehole depth is shallow at 9.3 m below ground level.

Figure 11 shows the temporal variation in inorganic chemical composition of streamwater from the Fylde. The plot shows the less frequent sampling of the streamwaters over the phase of reporting. It also shows the large variability over time in streamwater inorganic compositions and the lack of clear evidence for temporal trends. The variability is likely most responsive to varying rainfall and stream discharge.

Figure 12 shows the temporal variation in groundwater inorganic chemistry from boreholes at the PNR site. For each analyte shown, upper plots illustrate BGS-analysed data and lower plots, data analysed by Cuadrilla consultants. Borehole naming conventions and symbols differ but colours are consistent between investigating organisation (e.g. Site C 55 = Site BH01A).

The groundwater data for PNR analysed by BGS show a time range from May 2017 to March 2020, after which site access was not possible. PNR water-quality monitoring for the current project phase therefore necessarily lacks BGS data. The Cuadrilla data show a time range from July 2016 to June 2020. No data were available in the public domain after that time[1], although it is unclear whether any further sampling and analysis has taken place subsequently. Data for Cuadrilla groundwater sampling for June 2020, reported on the Environment Agency website[1], also encompassed a more restricted range of analytes (Ca, Na, K, Cl, CH_4, Cd, Ba, Sr, Zn) compared to previous monitoring rounds. The revised environmental permit approved a reduction in groundwater and surface-water monitoring frequency to quarterly and with a reduced range of analytes (Environment Agency, 2019, 2020).

From visual inspection, neither the BGS data nor the Cuadrilla data showed any clear evidence of consistent trends in concentrations over the time interval when hydraulic fracturing at PNR took place or subsequently, albeit the time range of investigation post fracturing is curtailed.

[1]Data downloaded from the Environment Agency website: https://consult.environment-agency.gov.uk/onshore-oil-and-gas/information-on-cuadrillas-preston-new-road-site/
No data could be acquired from the Cuadrilla eportal: https://www.cuadrillaresourceseportal.com/

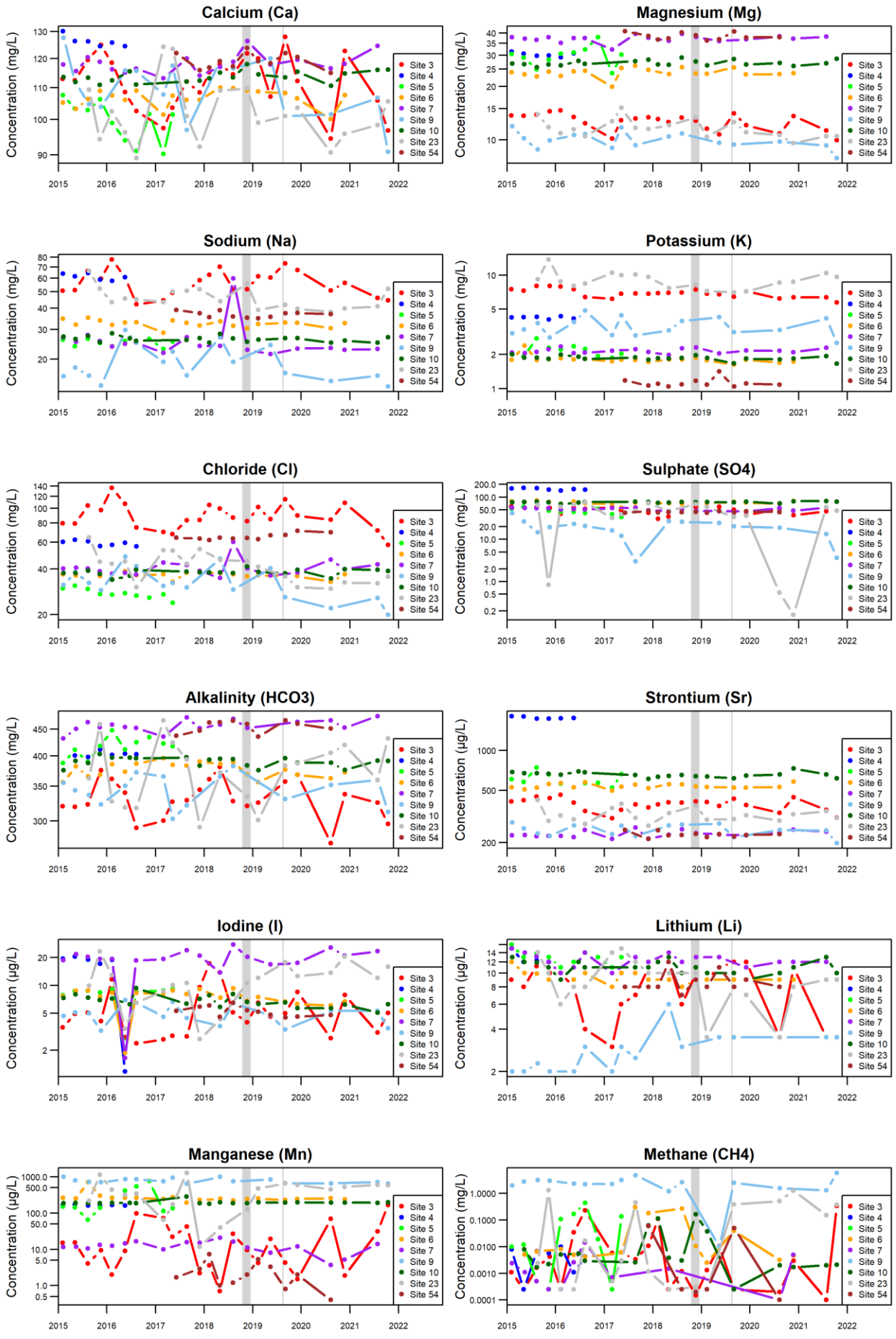

Figure 9. Temporal variation in groundwater chemical compositions from third-party boreholes in the Superficial aquifer in the Fylde. Intervals of hydraulic fracturing denoted by grey bars

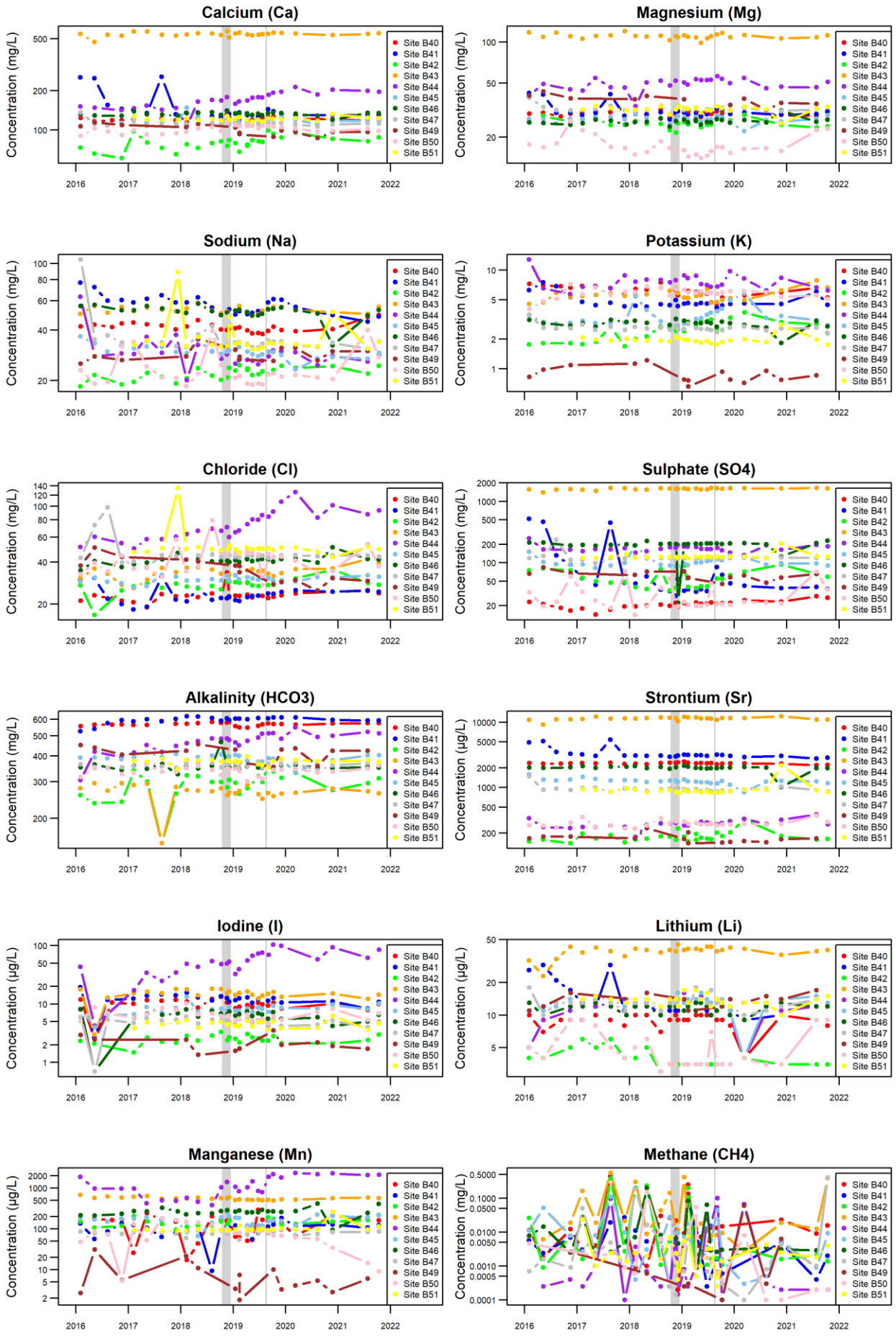

Figure 10. Temporal variation in groundwater chemical compositions, BGS boreholes, in the Superficial aquifer in the Fylde. Intervals of hydraulic fracturing denoted by grey bars

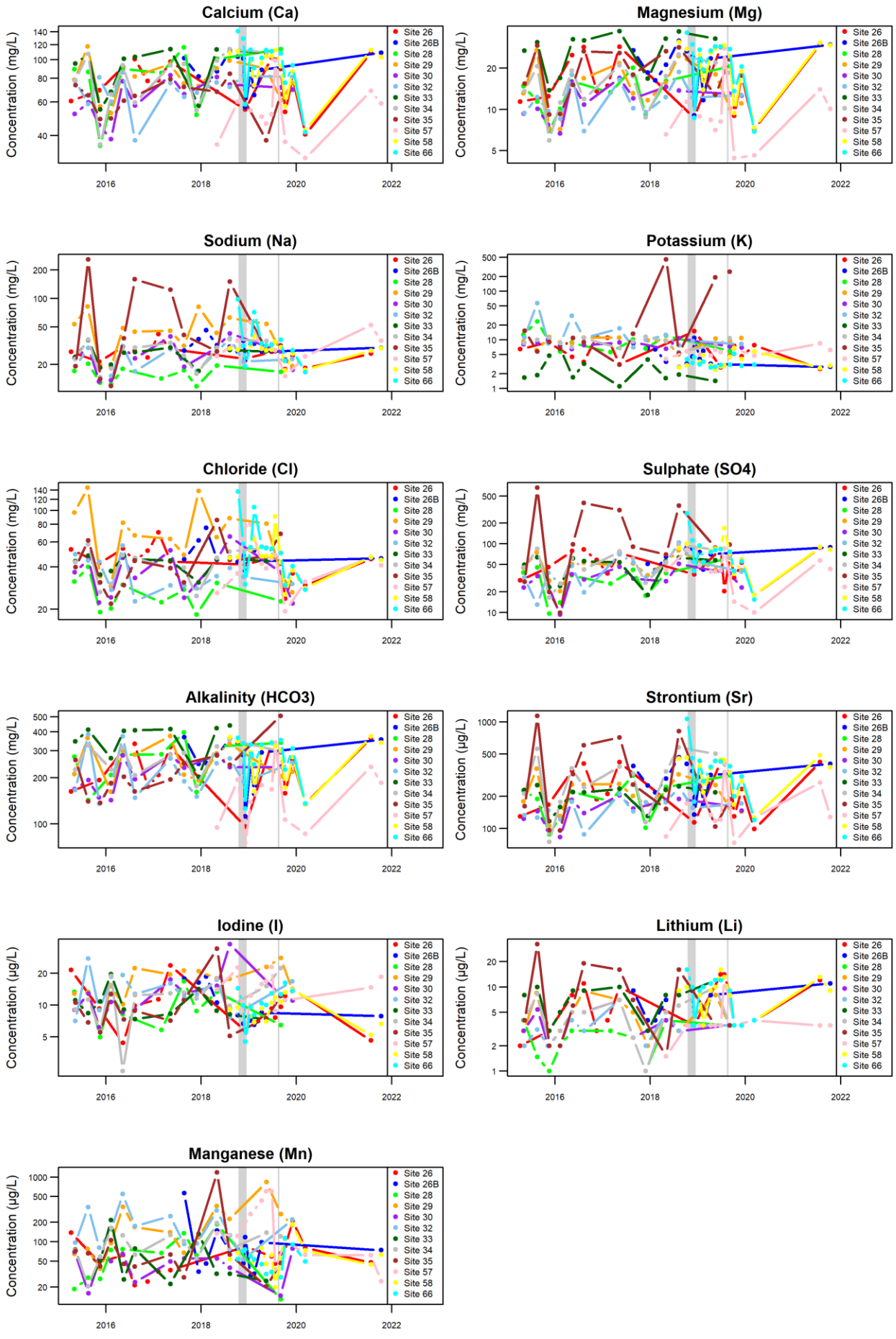

Figure 11. Temporal variation in streamwater chemical compositions from the monitoring network in the Fylde. Intervals of hydraulic fracturing denoted by grey bars

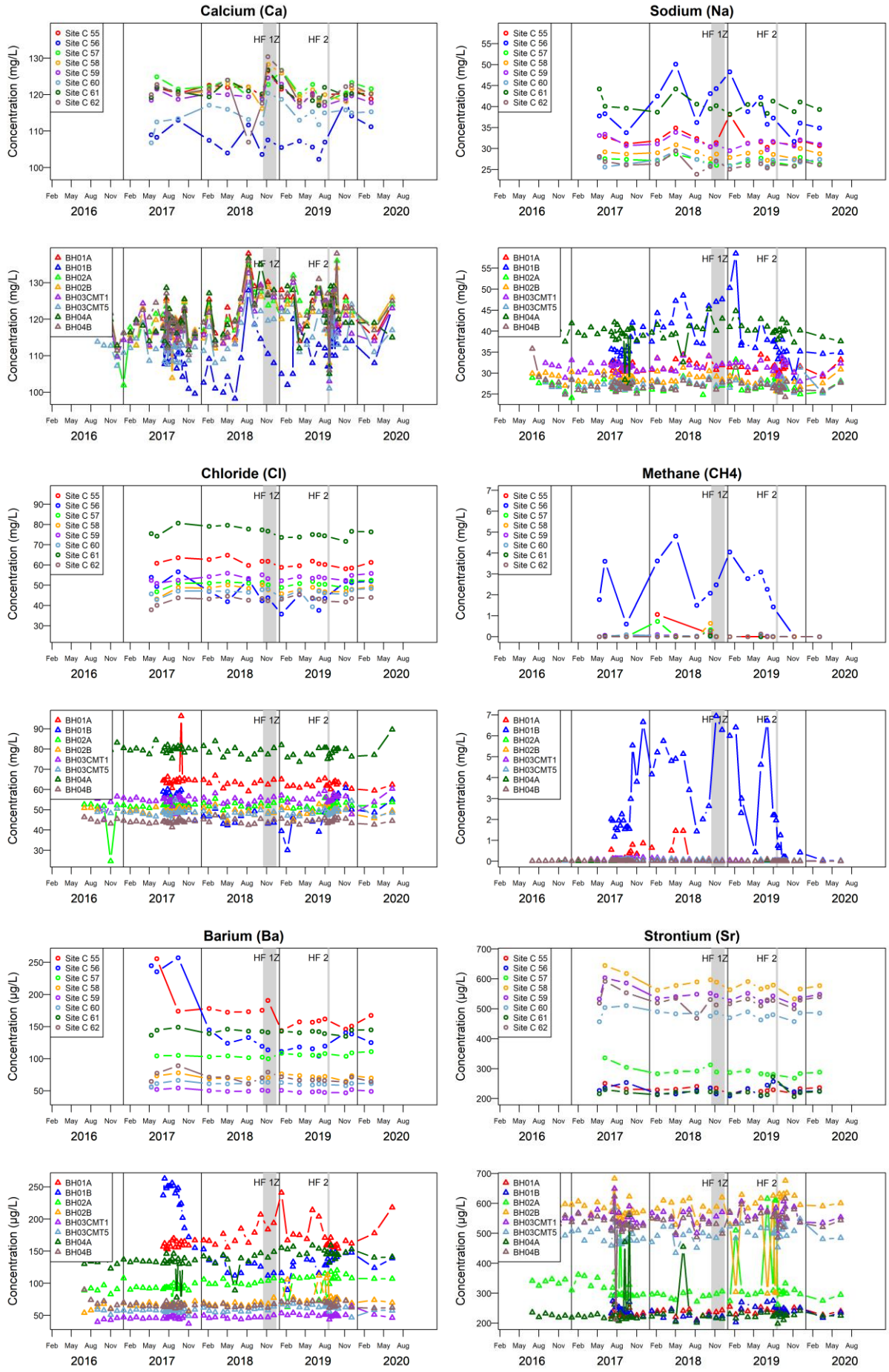

Figure 12. Variation in selected analytes from PNR groundwater boreholes. Top figures: BGS data, bottom figures: Cuadrilla data (Environment Agency website: © Environment Agency, 2020, released under Open Government Licence 3.0). Grey bars: as previous figs

3.3 STATISTICAL EVALUATION

Establishing the baseline in groundwater quality as a means to distinguish any changes caused by subsurface activities has been an important objective of the monitoring programme. A statistical approach to detecting change in groundwater-quality monitoring data under baseline and operational (post-baseline) conditions has been developed in previous phases of the monitoring programme and the methodology reported by Ward et al. (2019) and its preliminary application to the Vale of Pickering by Ward et al. (2020).

The approach involves assessment of the statistical distributions and variations in different groundwater monitoring rounds. Modelling of the data involves accounting for variation, including spatial and temporal correlation, under baseline conditions, to establish the variation that would be expected for a given solute under operational conditions in the absence of any changes post-baseline. This is then compared with the observed post-baseline variation. Data are log-transformed where necessary to provide a distribution closer to the normal distribution. Individual site data are standardised by subtracting the site mean and dividing by the site standard deviation. The model determines the expected standardised mean value for a given round of sampling and its confidence limits. The model can account for sites not being sampled on every sample round (Ward et al., 2019).

Ward et al. (2019) used sequences of baseline monitoring data from the Vale of Pickering to investigate the number of sample rounds needed to establish the standardised baseline mean to within acceptable confidence limits. The modelling suggested that for the Pickering data, around 30 rounds of monitoring were required to capture the expected variation in the groundwater measurements, with fewer rounds resulting in increased numbers of false positives (outside the 95% confidence intervals).

Accessibility of data processing has been approached by development of an app in R Shiny (Ward et al., 2020). The approach has been used here to assess the spatial and temporal data for groundwater from the Quaternary aquifer in the Fylde during the baseline and post-baseline periods. The approach aims to identify rounds of post-baseline sampling where the standardised mean appears to be inconsistent with the baseline.

As described in the methodology, log-transforms were used wherever the histograms of standardised values looked closer to the normal distribution with the transform than without. This transformation to a distribution closer to normal is noted as (log) in R Shiny outputs (Sections 3.3.1 and 3.3.2). Non-detects in the data are set to half of the detection limit.

For the Lancashire data, two sets of statistical analyses on differing spatial scales have been performed. The first was for groundwater samples from boreholes in Quaternary deposits across the Fylde (third-party boreholes in the monitoring network, BGS boreholes and Cuadrilla (PNR) boreholes). The second was for boreholes in the Cuadrilla PNR suite only (all BGS analyses).

For the purpose of change detection, the baseline period for groundwater quality across the Fylde is taken to have ended on 14-10-2018, the day before the first hydraulic fracture of borehole 1Z (although 11-10-2018 was the closest selectable water sampling date). Log-transforms are applied to the same analytes in the PNR dataset as in the full data results.

In the dataset, up to 15 rounds of baseline data are available for any single site, up to 9 for the PNR sites. This is less than the estimated number of 30 monitoring rounds suggested to be needed for the Vale of Pickering baseline dataset (Ward et al. 2019). While these data are not directly comparable, the finding suggests caution is warranted in assuming adequate characterisation of the baseline from the data available.

Results are shown for the evaluation of all sites for a number of analytes in groundwater from the Quaternary network of Fylde in Section 3.3.1 and for groundwater from PNR in

Section 3.3.2. Analytes are chosen as those with mostly detectable values and demonstrating certain behaviour (e.g. indicators of salinity, redox and dissolved-gas content). Plots show the deviations from the 95th percent confidence intervals and 3σ ranges (99.7% confidence) around the standardised mean. Confidence bands (detailed in Ward et al., 2019) vary according to numbers of samples per sampling round; bands were larger in some of the earlier rounds due to smaller numbers of sampled sites.

For all locations (Section 3.3.1), data show values above the 95% confidence limit for a number of sites for SEC, Sites B44 and B50 and some PNR sites for a short post-baseline period for Ca, Sites B42 and B48 for Na, Site B 42 for K, Site B44 and B48 for Cl, Site B48 for SO_4, Sites B42 and B44 for Br and Sites B50 and B51 for Ba. A few sites also showed occasional values below the 95% confidence limits: Site B51 for NH_4, Sites B40 and B41 for Na and Sites B40 and B48 for K. For dissolved CH_4, for sites outside the confidence band, more sites showed values below than above the 95% confidence limit. Sites B42 and B44 were from the Roseacre borehole cluster. Site B44 was the site identified as showing significant temporal variations in Section 3.2.

For the PNR-only data (Section 3.3.2), Site C 58 is periodically above the 95% confidence limit for NH_4 and Site C 57 for Ba. As for the larger area, dissolved CH_4 values were more often below the 95% confidence interval than above. Otherwise, many fewer values outwith the limits were found.

Strongest evidence for significant post-baseline differences in chemistry would likely manifest in consistent outside of 95% limits in solutes of similar behaviour in given samples (e.g. consistent exceedances for Na, Cl, SO_4 as indicators of increased salinity). Given relatively uniform hydrogeological conditions, consistency in solutes of similar behaviour across sites might also be expected. The data do not show consistency in values outside the 95% confidence limits and these are suspected to be falsely flagging data as inconsistent with the baseline, attributed to the limitations caused by the large spatial variability in analyses and potentially the limited numbers of monitoring rounds.

Further investigation could be carried out to assess statistical distributions at different spatial and temporal scales to investigate their impacts on the standardised means, confidence intervals and observed deviations.

Choosing the end of the baseline period as the last sampling date before the first hydraulic fracture is logical, though any impacts of operations at >1 km depth is unlikely to produce immediate responses at superficial levels unless arising from surface processes (e.g. spills) or direct leakage via the gas well. Any impacts in boreholes further afield from PNR would likely take longer to manifest and need a longer period to monitor.

3.3.1 All locations

SEC (µS/cm)	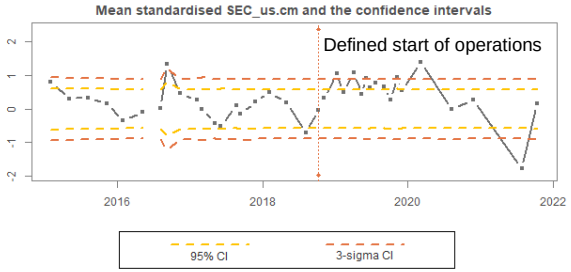 The fitted model has an overall mean of 0.039. The estimated standard deviation of the model residual is 0.288 and the estimated standard deviation of temporal random effect is 0.898. The ratio of random variation over total variation is 0.5. The baseline model provides a measure of the overall performance of all sampling sites. Among the averaged (across sites) standardised data in the testing period, 9 out of 17 values fall out of the 95% confidence intervals, and 6 fall out of the three times standard deviation confidence interval.	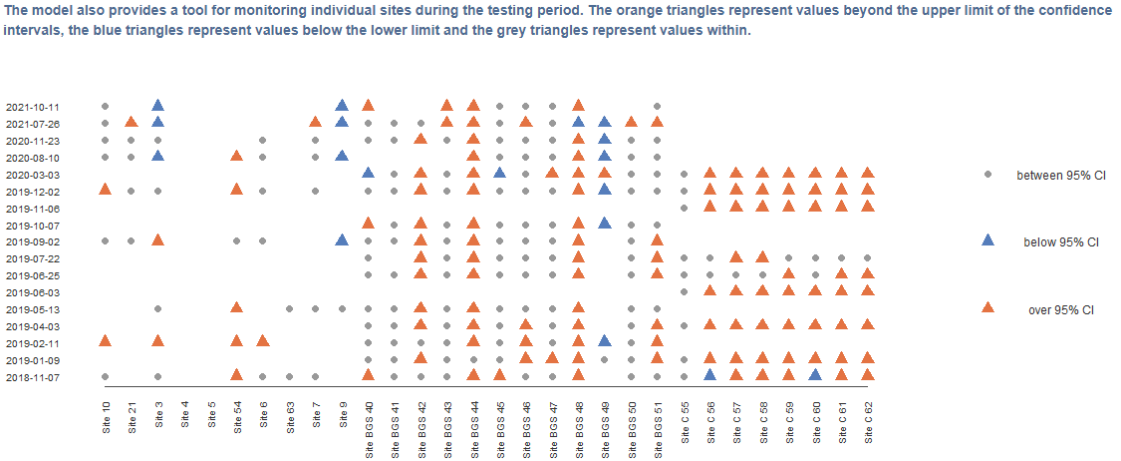
HCO_3 (mg/L) (log)	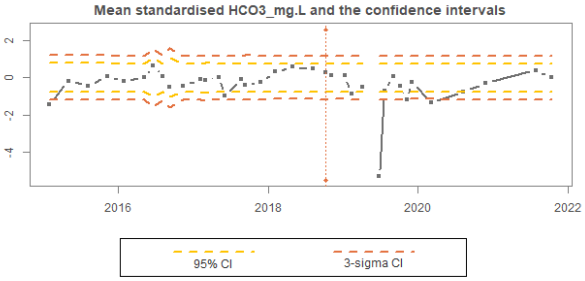 The fitted model has an overall mean of -0.102. The estimated standard deviation of the model residual is 0.376 and the estimated standard deviation of temporal random effect is 0.878. The ratio of random variation over total variation is 0.5. The baseline model provides a measure of the overall performance of all sampling sites. Among the averaged (across sites) standardised data in the testing period, NA out of 17 values fall out of the 95% confidence intervals, and NA fall out of the three times standard deviation confidence interval.	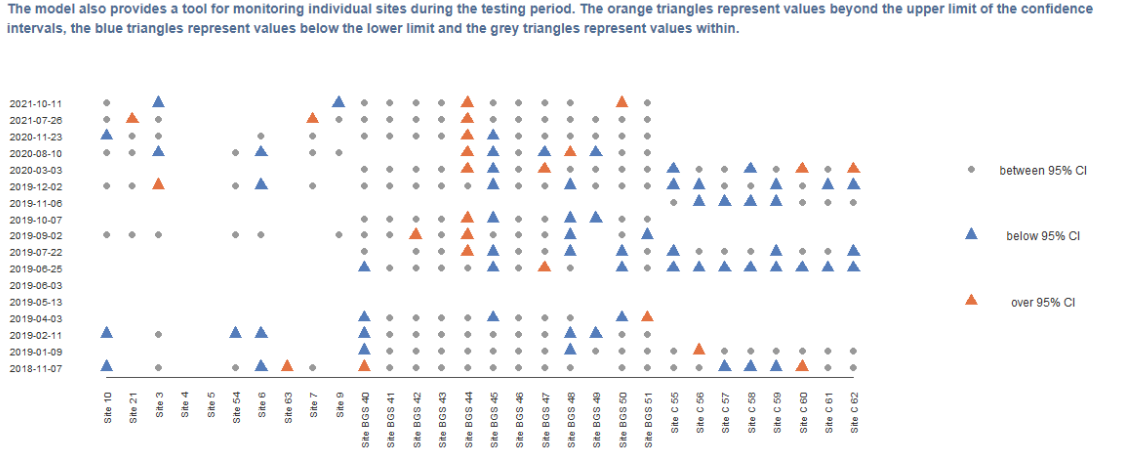

NH_4 (mg/L) (log)	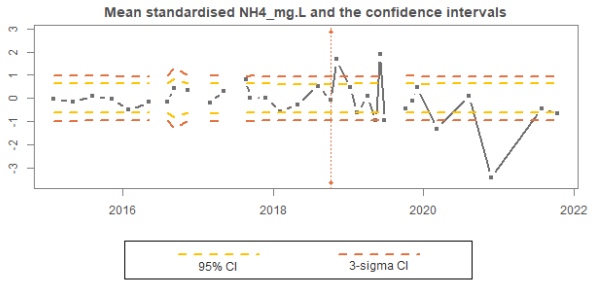 The fitted model has an overall mean of 0.001. The estimated standard deviation of the model residual is 0.307 and the estimated standard deviation of temporal random effect is 0.881. The ratio of random variation over total variation is 0.5. The baseline model provides a measure of the overall performance of all sampling sites. Among the averaged (across sites) standardised data in the testing period, NA out of 17 values fall out of the 95% confidence intervals, and NA fall out of the three times standard deviation confidence interval.	The model also provides a tool for monitoring individual sites during the testing period. The orange triangles represent values beyond the upper limit of the confidence intervals, the blue triangles represent values below the lower limit and the grey triangles represent values within. 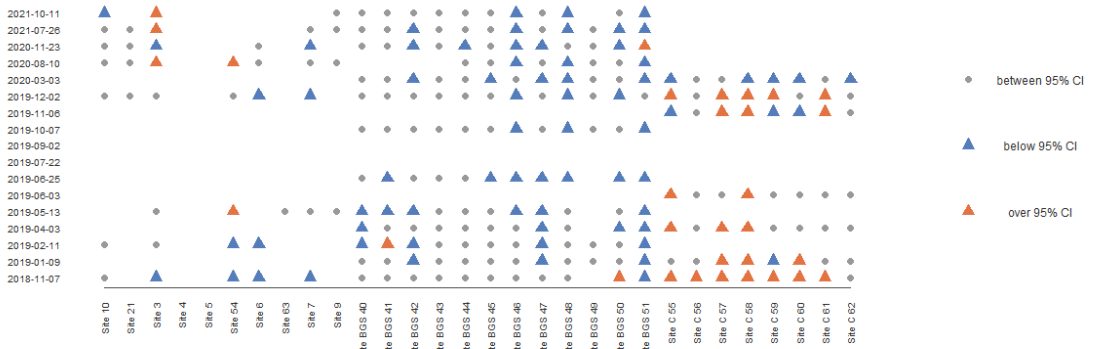
Ca (mg/L) (log)	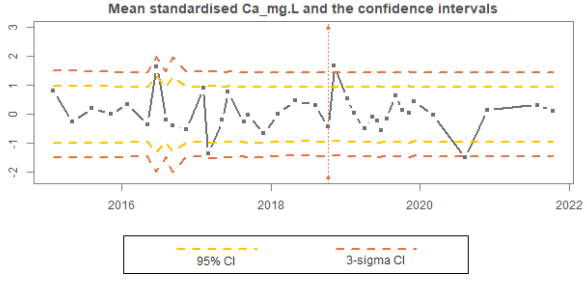 The fitted model has an overall mean of 0.001. The estimated standard deviation of the model residual is 0.469 and the estimated standard deviation of temporal random effect is 0.851. The ratio of random variation over total variation is 0.5. The baseline model provides a measure of the overall performance of all sampling sites. Among the averaged (across sites) standardised data in the testing period, 2 out of 17 values fall out of the 95% confidence intervals, and 2 fall out of the three times standard deviation confidence interval.	The model also provides a tool for monitoring individual sites during the testing period. The orange triangles represent values beyond the upper limit of the confidence intervals, the blue triangles represent values below the lower limit and the grey triangles represent values within. 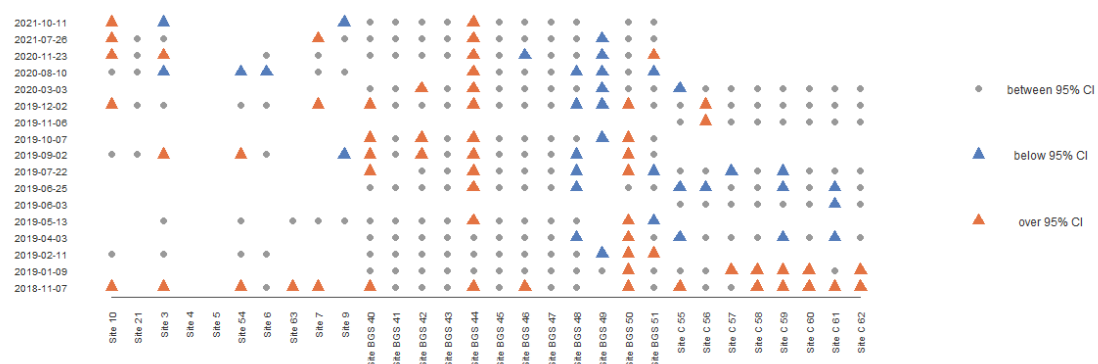

Mg (mg/L)	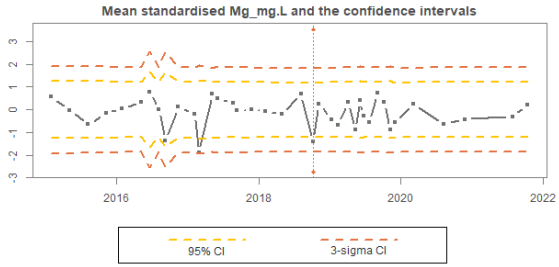 The fitted model has an overall mean of -0.074. The estimated standard deviation of the model residual is 0.601 and the estimated standard deviation of temporal random effect is 0.764. The ratio of random variation over total variation is 0.5. The baseline model provides a measure of the overall performance of all sampling sites. Among the averaged (across sites) standardised data in the testing period, 0 out of 17 values fall out of the 95% confidence intervals, and 0 fall out of the three times standard deviation confidence interval.	The model also provides a tool for monitoring individual sites during the testing period. The orange triangles represent values beyond the upper limit of the confidence intervals, the blue triangles represent values below the lower limit and the grey triangles represent values within. 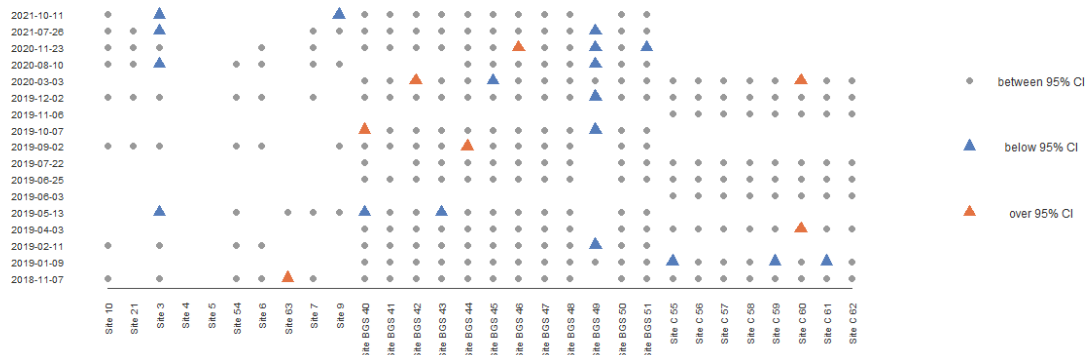
Na (mg/L) (log)	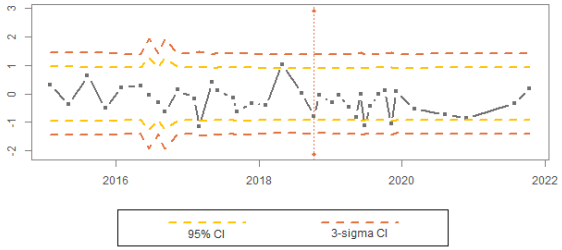 The fitted model has an overall mean of -0.072. The estimated standard deviation of the model residual is 0.454 and the estimated standard deviation of temporal random effect is 0.823. The ratio of random variation over total variation is 0.5. The baseline model provides a measure of the overall performance of all sampling sites. Among the averaged (across sites) standardised data in the testing period, 2 out of 17 values fall out of the 95% confidence intervals, and 0 fall out of the three times standard deviation confidence interval.	The model also provides a tool for monitoring individual sites during the testing period. The orange triangles represent values beyond the upper limit of the confidence intervals, the blue triangles represent values below the lower limit and the grey triangles represent values within. 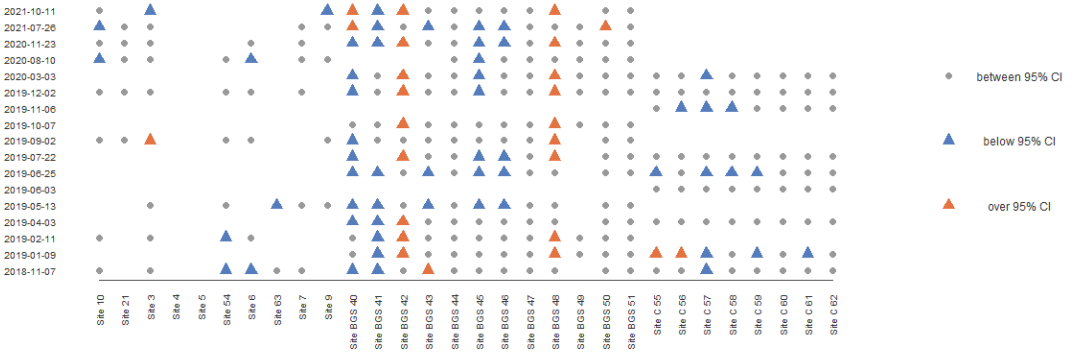

K (mg/L) (log)	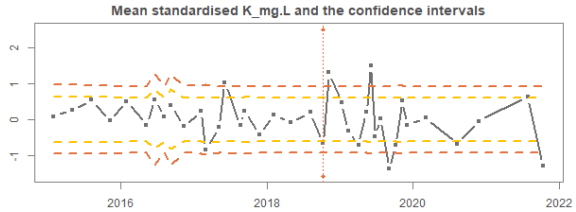 The fitted model has an overall mean of 0.023. The estimated standard deviation of the model residual is 0.3 and the estimated standard deviation of temporal random effect is 0.904. The ratio of random variation over total variation is 0.5. The baseline model provides a measure of the overall performance of all sampling sites. Among the averaged (across sites) standardised data in the testing period, 8 out of 17 values fall out of the 95% confidence intervals, and 4 fall out of the three times standard deviation confidence interval.	The model also provides a tool for monitoring individual sites during the testing period. The orange triangles represent values beyond the upper limit of the confidence intervals, the blue triangles represent values below the lower limit and the grey triangles represent values within. 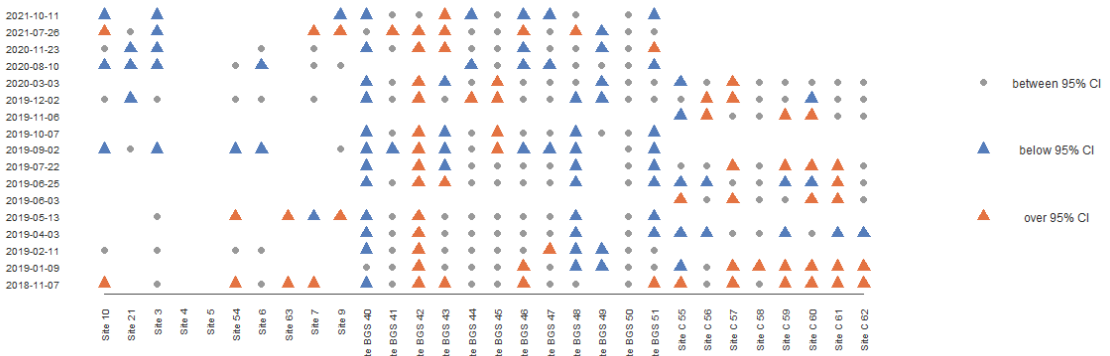
Cl (mg/L)	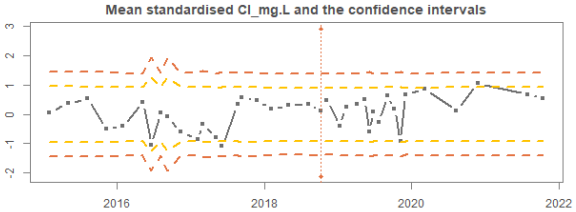 The fitted model has an overall mean of -0.053. The estimated standard deviation of the model residual is 0.453 and the estimated standard deviation of temporal random effect is 0.845. The ratio of random variation over total variation is 0.5. The baseline model provides a measure of the overall performance of all sampling sites. Among the averaged (across sites) standardised data in the testing period, 1 out of 17 values fall out of the 95% confidence intervals, and 0 fall out of the three times standard deviation confidence interval.	The model also provides a tool for monitoring individual sites during the testing period. The orange triangles represent values beyond the upper limit of the confidence intervals, the blue triangles represent values below the lower limit and the grey triangles represent values within. 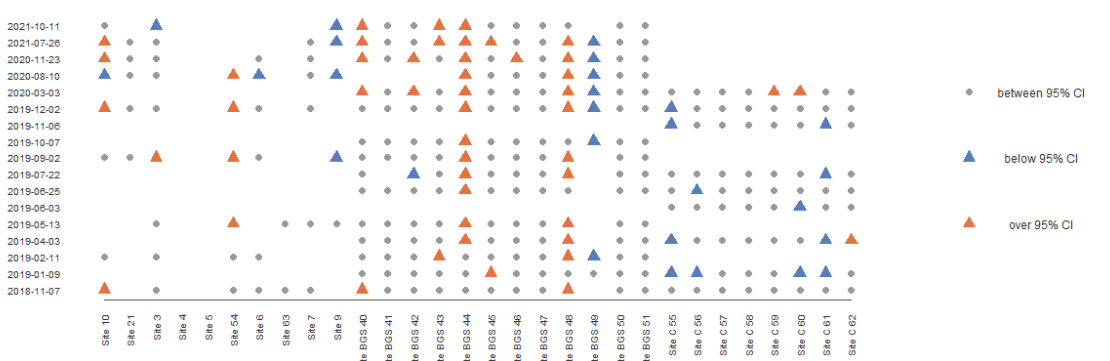

SO_4 (mg/L) (log)	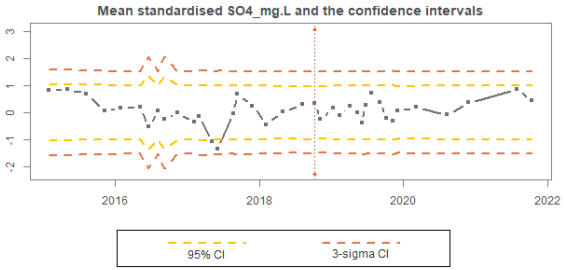 The fitted model has an overall mean of 0.031. The estimated standard deviation of the model residual is 0.489 and the estimated standard deviation of temporal random effect is 0.832. The ratio of random variation over total variation is 0.5. The baseline model provides a measure of the overall performance of all sampling sites. Among the averaged (across sites) standardised data in the testing period, 0 out of 17 values fall out of the 95% confidence intervals, and 0 fall out of the three times standard deviation confidence interval.	The model also provides a tool for monitoring individual sites during the testing period. The orange triangles represent values beyond the upper limit of the confidence intervals, the blue triangles represent values below the lower limit and the grey triangles represent values within. 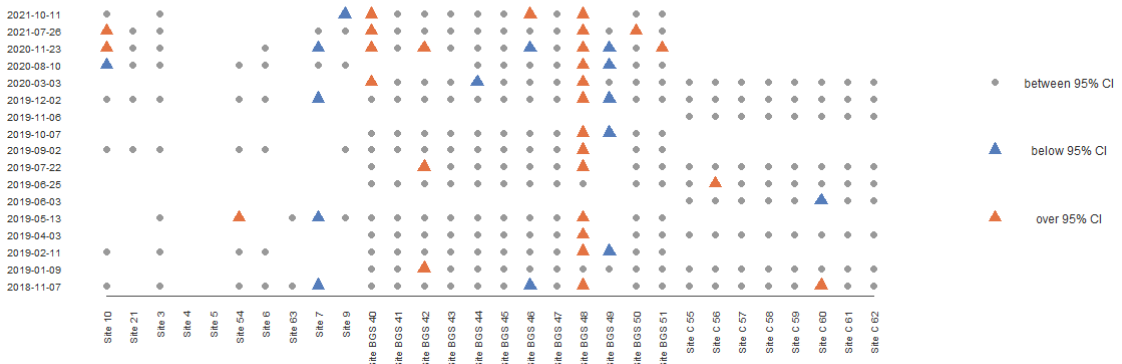
Br (mg/L)	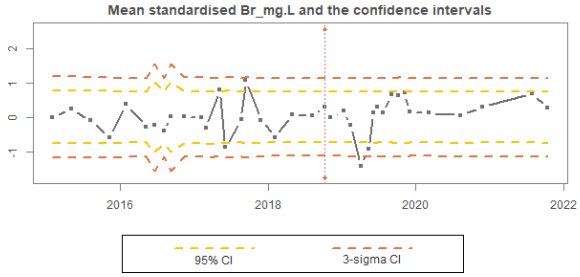 The fitted model has an overall mean of -0.018. The estimated standard deviation of the model residual is 0.368 and the estimated standard deviation of temporal random effect is 0.879. The ratio of random variation over total variation is 0.5. The baseline model provides a measure of the overall performance of all sampling sites. Among the averaged (across sites) standardised data in the testing period, 2 out of 17 values fall out of the 95% confidence intervals, and 1 fall out of the three times standard deviation confidence interval.	The model also provides a tool for monitoring individual sites during the testing period. The orange triangles represent values beyond the upper limit of the confidence intervals, the blue triangles represent values below the lower limit and the grey triangles represent values within. 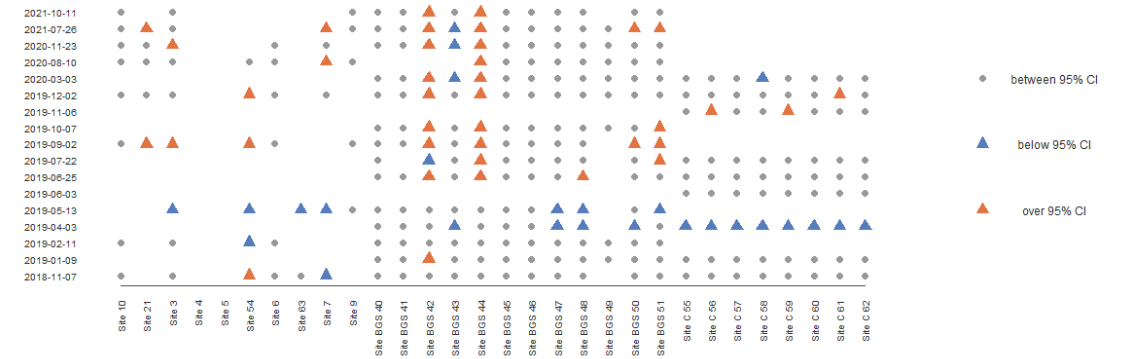

Ba (µg/L) (log)	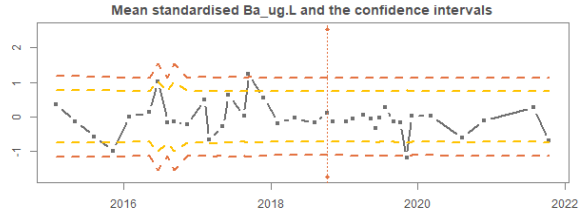 The fitted model has an overall mean of 0.016. The estimated standard deviation of the model residual is 0.364 and the estimated standard deviation of temporal random effect is 0.894. The ratio of random variation over total variation is 0.5. The baseline model provides a measure of the overall performance of all sampling sites. Among the averaged (across sites) standardised data in the testing period, 1 out of 17 values fall out of the 95% confidence intervals, and 1 fall out of the three times standard deviation confidence interval.	The model also provides a tool for monitoring individual sites during the testing period. The orange triangles represent values beyond the upper limit of the confidence intervals, the blue triangles represent values below the lower limit and the grey triangles represent values within. 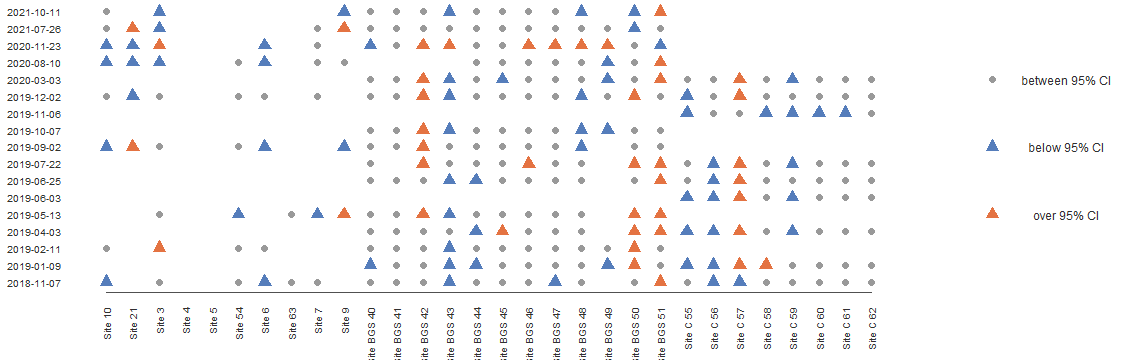
Li (µg/L)	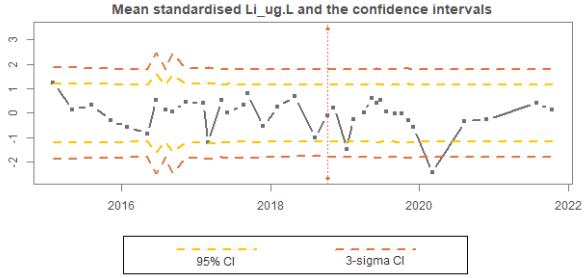 The fitted model has an overall mean of 0.049. The estimated standard deviation of the model residual is 0.578 and the estimated standard deviation of temporal random effect is 0.751. The ratio of random variation over total variation is 0.5. The baseline model provides a measure of the overall performance of all sampling sites. Among the averaged (across sites) standardised data in the testing period, 2 out of 17 values fall out of the 95% confidence intervals, and 1 fall out of the three times standard deviation confidence interval.	The model also provides a tool for monitoring individual sites during the testing period. The orange triangles represent values beyond the upper limit of the confidence intervals, the blue triangles represent values below the lower limit and the grey triangles represent values within. 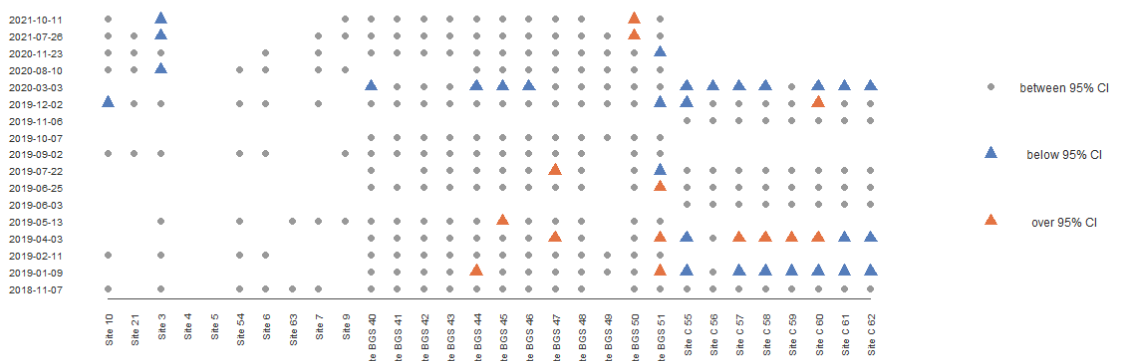

CH_4 (µg/L) (log)	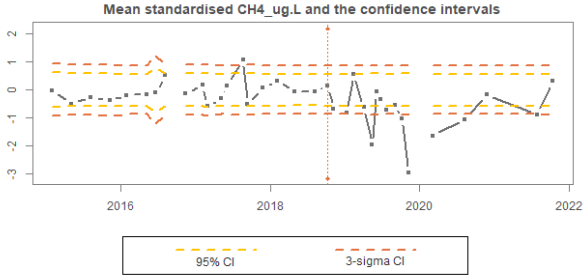 The fitted model has an overall mean of -0.017. The estimated standard deviation of the model residual is 0.284 and the estimated standard deviation of temporal random effect is 0.899. The ratio of random variation over total variation is 0.5. The baseline model provides a measure of the overall performance of all sampling sites. Among the averaged (across sites) standardised data in the testing period, NA out of 17 values fall out of the 95% confidence intervals, and NA fall out of the three times standard deviation confidence interval.	The model also provides a tool for monitoring individual sites during the testing period. The orange triangles represent values beyond the upper limit of the confidence intervals, the blue triangles represent values below the lower limit and the grey triangles represent values within. 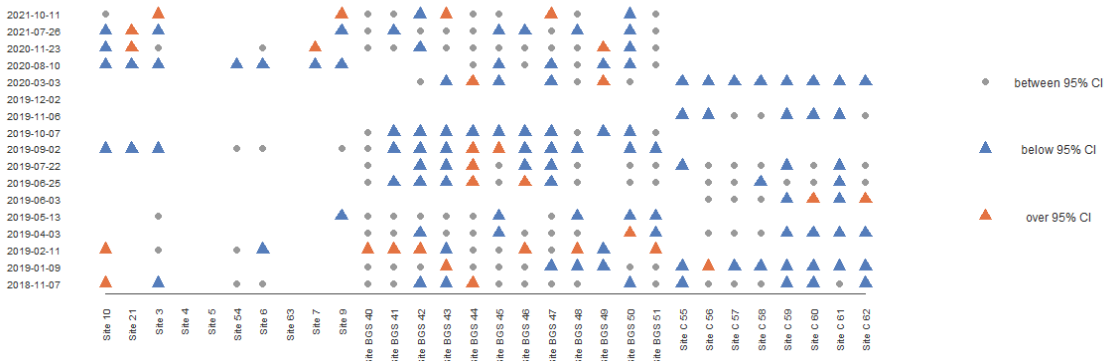

3.3.2 Preston New Road site

SEC (µS/cm)	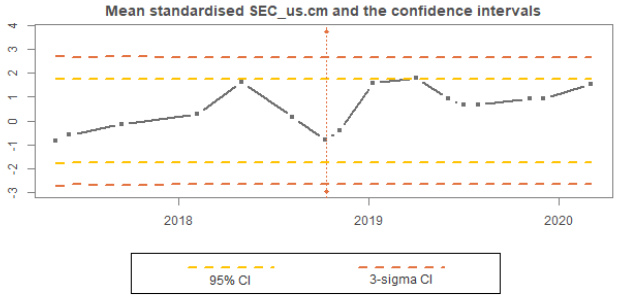 The fitted model has an overall mean of -0.045. The estimated standard deviation of the model residual is 0.841 and the estimated standard deviation of temporal random effect is 0.484. The ratio of random variation over total variation is 0.5. The baseline model provides a measure of the overall performance of all sampling sites. Among the averaged (across sites) standardised data in the testing period, 1 out of 9 values fall out of the 95% confidence intervals, and 0 fall out of the three times standard deviation confidence interval.	The model also provides a tool for monitoring individual sites during the testing period. The orange triangles represent values beyond the upper limit of the confidence intervals, the blue triangles represent values below the lower limit and the grey triangles represent values within. 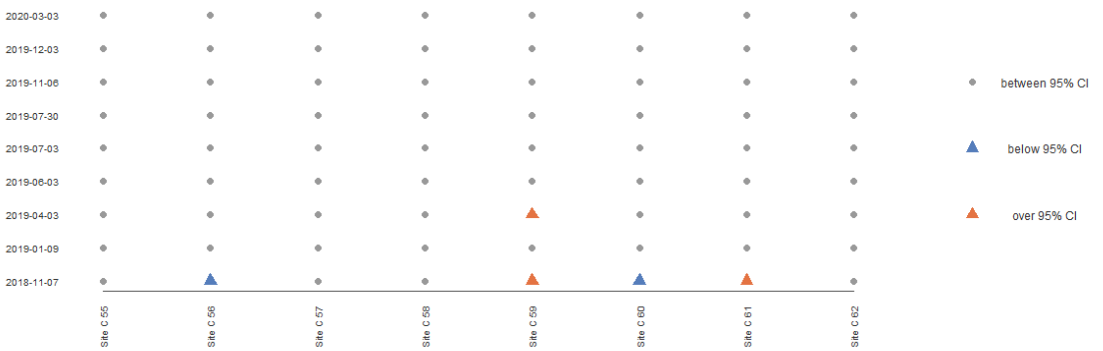

HCO_3 (mg/L) (log)	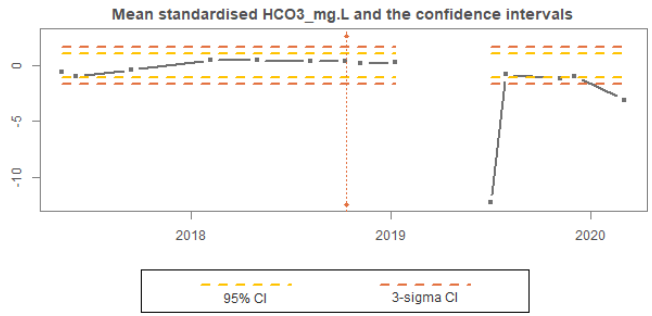 The fitted model has an overall mean of -0.02. The estimated standard deviation of the model residual is 0.513 and the estimated standard deviation of temporal random effect is 0.797. The ratio of random variation over total variation is 0.5. The baseline model provides a measure of the overall performance of all sampling sites. Among the averaged (across sites) standardised data in the testing period, NA out of 9 values fall out of the 95% confidence intervals, and NA fall out of the three times standard deviation confidence interval.	The model also provides a tool for monitoring individual sites during the testing period. The orange triangles represent values beyond the upper limit of the confidence intervals, the blue triangles represent values below the lower limit and the grey triangles represent values within. 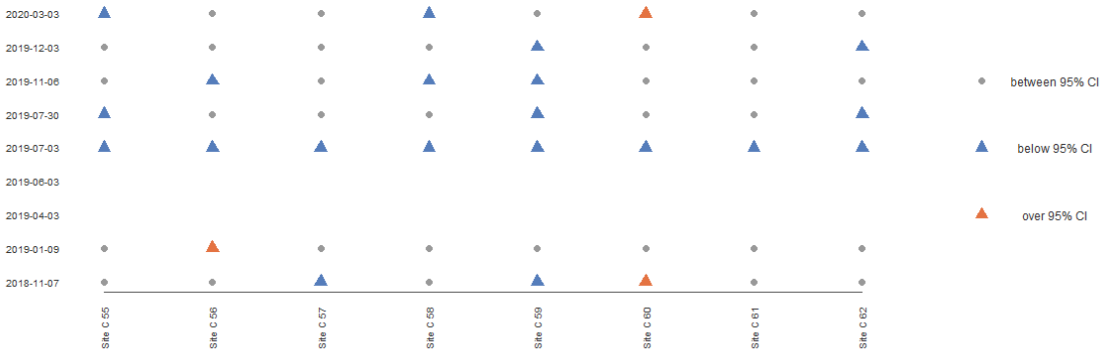
NH_4 (mg/L) (log)	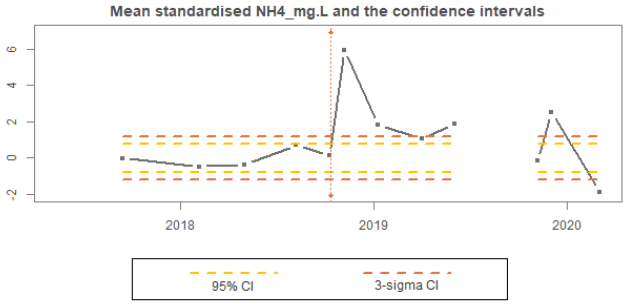 The fitted model has an overall mean of 0.002. The estimated standard deviation of the model residual is 0.366 and the estimated standard deviation of temporal random effect is 0.835. The ratio of random variation over total variation is 0.5. The baseline model provides a measure of the overall performance of all sampling sites. Among the averaged (across sites) standardised data in the testing period, NA out of 9 values fall out of the 95% confidence intervals, and NA fall out of the three times standard deviation confidence interval.	The model also provides a tool for monitoring individual sites during the testing period. The orange triangles represent values beyond the upper limit of the confidence intervals, the blue triangles represent values below the lower limit and the grey triangles represent values within. 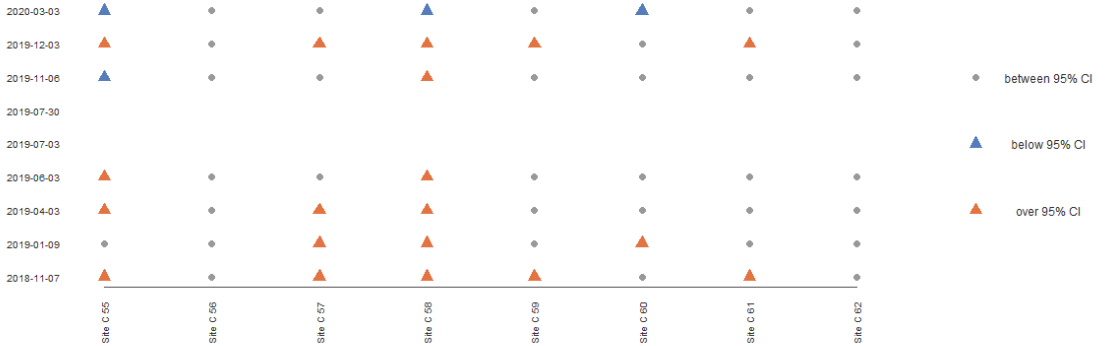

Ca (mg/L) (log)	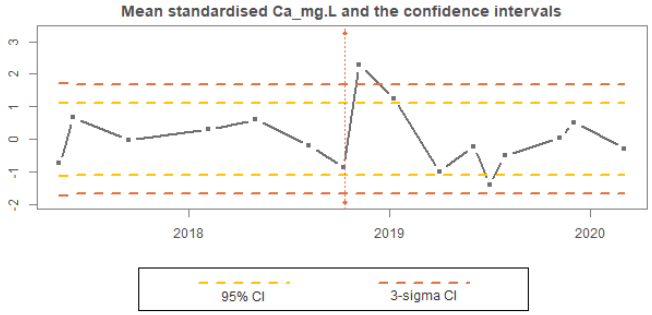 The fitted model has an overall mean of -0.028. The estimated standard deviation of the model residual is 0.531 and the estimated standard deviation of temporal random effect is 0.79. The ratio of random variation over total variation is 0.5. The baseline model provides a measure of the overall performance of all sampling sites. Among the averaged (across sites) standardised data in the testing period, 3 out of 9 values fall out of the 95% confidence intervals, and 1 fall out of the three times standard deviation confidence interval.	The model also provides a tool for monitoring individual sites during the testing period. The orange triangles represent values beyond the upper limit of the confidence intervals, the blue triangles represent values below the lower limit and the grey triangles represent values within. 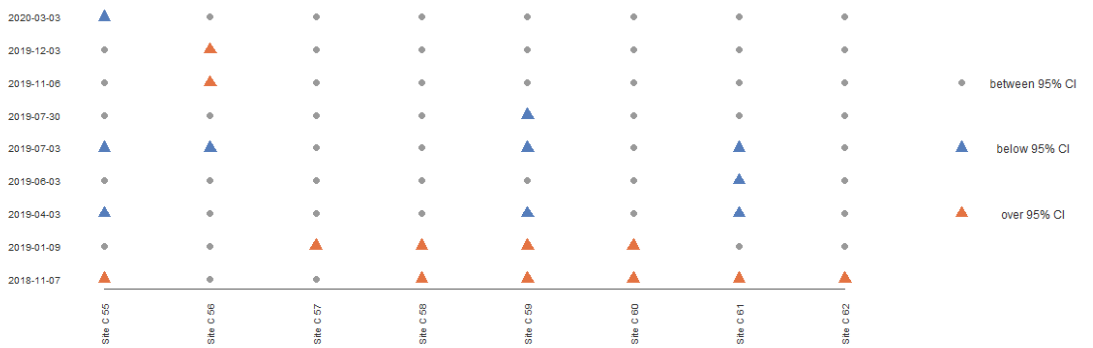
Mg (mg/L)	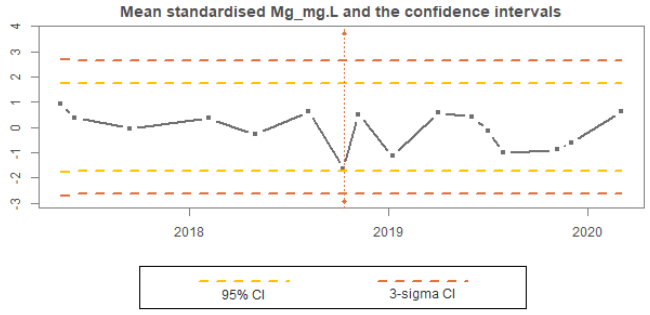 The fitted model has an overall mean of 0.047. The estimated standard deviation of the model residual is 0.833 and the estimated standard deviation of temporal random effect is 0.52. The ratio of random variation over total variation is 0.5. The baseline model provides a measure of the overall performance of all sampling sites. Among the averaged (across sites) standardised data in the testing period, 0 out of 9 values fall out of the 95% confidence intervals, and 0 fall out of the three times standard deviation confidence interval.	The model also provides a tool for monitoring individual sites during the testing period. The orange triangles represent values beyond the upper limit of the confidence intervals, the blue triangles represent values below the lower limit and the grey triangles represent values within. 

Na (mg/L) (log)	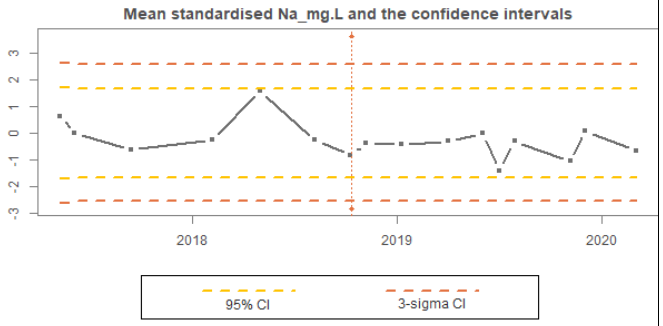 The fitted model has an overall mean of 0.031. The estimated standard deviation of the model residual is 0.806 and the estimated standard deviation of temporal random effect is 0.535. The ratio of random variation over total variation is 0.5. The baseline model provides a measure of the overall performance of all sampling sites. Among the averaged (across sites) standardised data in the testing period, 0 out of 9 values fall out of the 95% confidence intervals, and 0 fall out of the three times standard deviation confidence interval.	The model also provides a tool for monitoring individual sites during the testing period. The orange triangles represent values beyond the upper limit of the confidence intervals, the blue triangles represent values below the lower limit and the grey triangles represent values within. 
K (mg/L) (log)	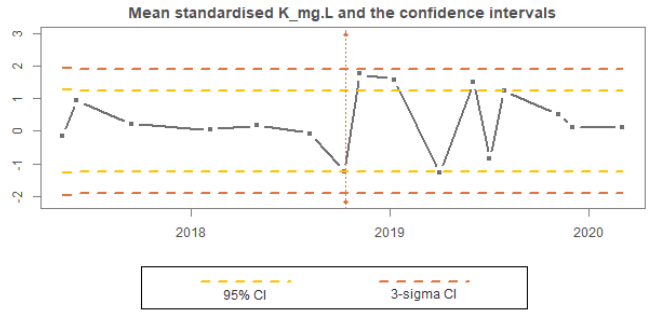 The fitted model has an overall mean of -0.006. The estimated standard deviation of the model residual is 0.601 and the estimated standard deviation of temporal random effect is 0.732. The ratio of random variation over total variation is 0.5. The baseline model provides a measure of the overall performance of all sampling sites. Among the averaged (across sites) standardised data in the testing period, 4 out of 9 values fall out of the 95% confidence intervals, and 0 fall out of the three times standard deviation confidence interval.	The model also provides a tool for monitoring individual sites during the testing period. The orange triangles represent values beyond the upper limit of the confidence intervals, the blue triangles represent values below the lower limit and the grey triangles represent values within. 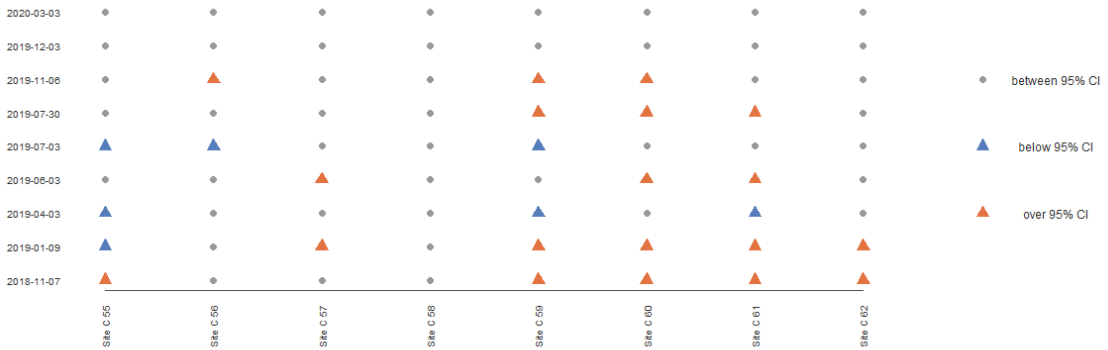

Cl (mg/L)	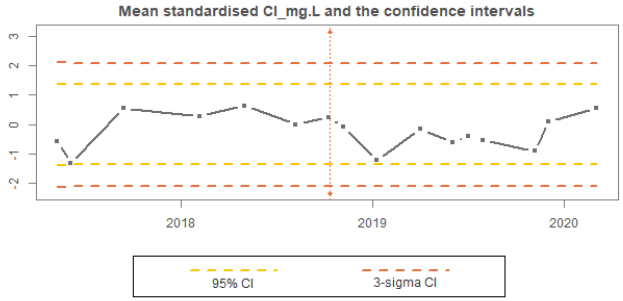 The fitted model has an overall mean of -0.026. The estimated standard deviation of the model residual is 0.659 and the estimated standard deviation of temporal random effect is 0.694. The ratio of random variation over total variation is 0.5. The baseline model provides a measure of the overall performance of all sampling sites. Among the averaged (across sites) standardised data in the testing period, 0 out of 9 values fall out of the 95% confidence intervals, and 0 fall out of the three times standard deviation confidence interval.	The model also provides a tool for monitoring individual sites during the testing period. The orange triangles represent values beyond the upper limit of the confidence intervals, the blue triangles represent values below the lower limit and the grey triangles represent values within. 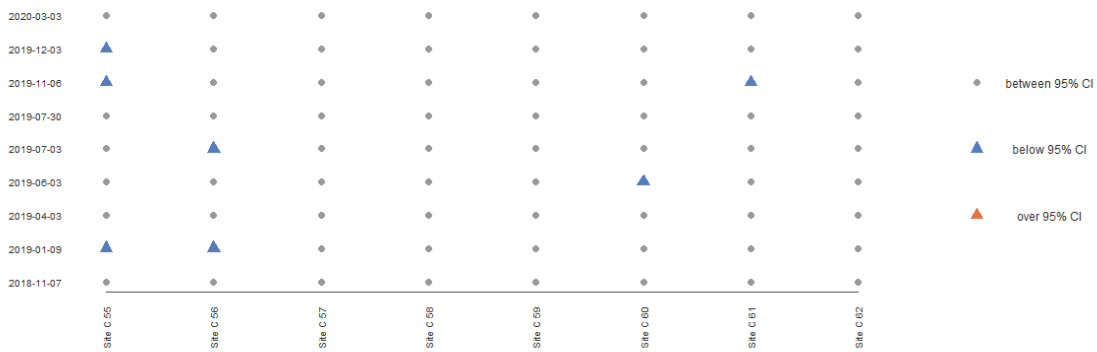
SO_4 (mg/L) (log)	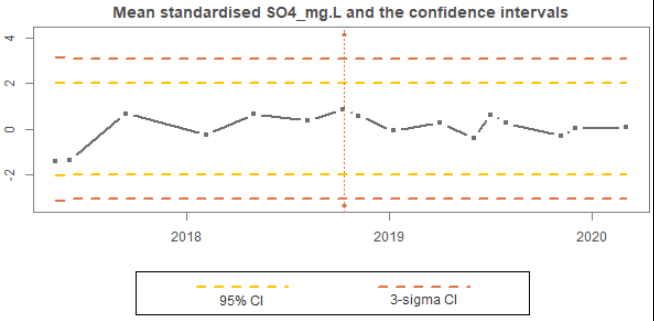 The fitted model has an overall mean of -0.076. The estimated standard deviation of the model residual is 0.971 and the estimated standard deviation of temporal random effect is 0.328. The ratio of random variation over total variation is 0.5. The baseline model provides a measure of the overall performance of all sampling sites. Among the averaged (across sites) standardised data in the testing period, 0 out of 9 values fall out of the 95% confidence intervals, and 0 fall out of the three times standard deviation confidence interval.	The model also provides a tool for monitoring individual sites during the testing period. The orange triangles represent values beyond the upper limit of the confidence intervals, the blue triangles represent values below the lower limit and the grey triangles represent values within. 

Br (mg/L)	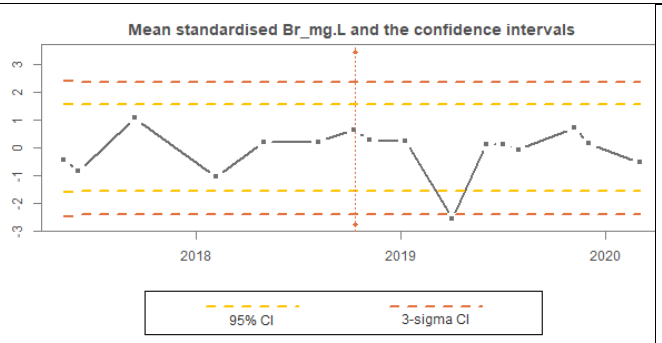 The fitted model has an overall mean of -0.021. The estimated standard deviation of the model residual is 0.747 and the estimated standard deviation of temporal random effect is 0.602. The ratio of random variation over total variation is 0.5. The baseline model provides a measure of the overall performance of all sampling sites. Among the averaged (across sites) standardised data in the testing period, 1 out of 9 values fall out of the 95% confidence intervals, and 1 fall out of the three times standard deviation confidence interval.	The model also provides a tool for monitoring individual sites during the testing period. The orange triangles represent values beyond the upper limit of the confidence intervals, the blue triangles represent values below the lower limit and the grey triangles represent values within. 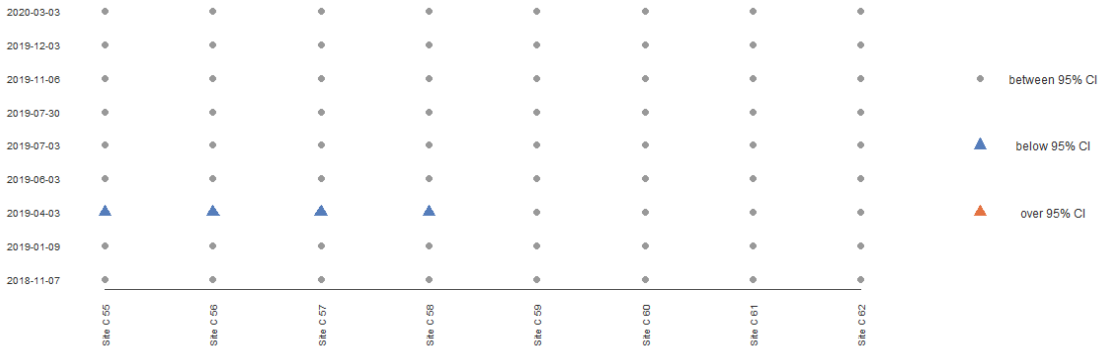
Ba (µg/L) (log)	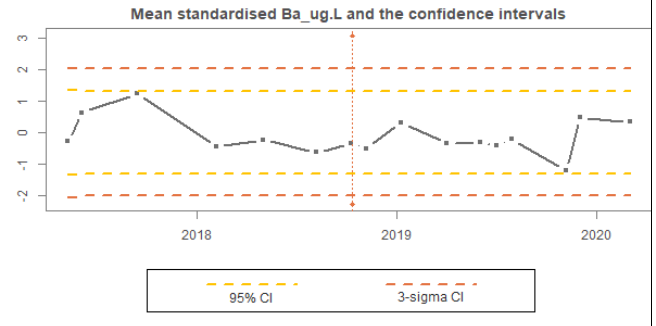 The fitted model has an overall mean of -0.012. The estimated standard deviation of the model residual is 0.633 and the estimated standard deviation of temporal random effect is 0.709. The ratio of random variation over total variation is 0.5. The baseline model provides a measure of the overall performance of all sampling sites. Among the averaged (across sites) standardised data in the testing period, 0 out of 9 values fall out of the 95% confidence intervals, and 0 fall out of the three times standard deviation confidence interval.	The model also provides a tool for monitoring individual sites during the testing period. The orange triangles represent values beyond the upper limit of the confidence intervals, the blue triangles represent values below the lower limit and the grey triangles represent values within. 

Li (µg/L)	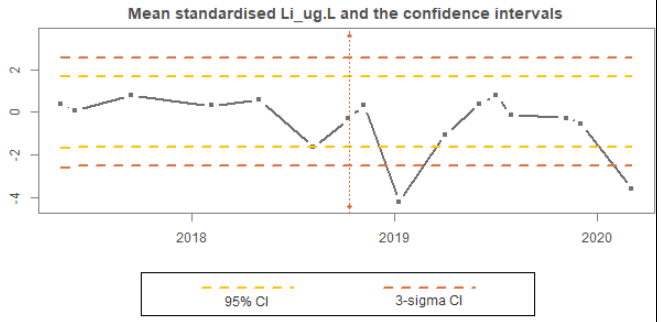 The fitted model has an overall mean of 0.019. The estimated standard deviation of the model residual is 0.793 and the estimated standard deviation of temporal random effect is 0.542. The ratio of random variation over total variation is 0.5. The baseline model provides a measure of the overall performance of all sampling sites. Among the averaged (across sites) standardised data in the testing period, 2 out of 9 values fall out of the 95% confidence intervals, and 2 fall out of the three times standard deviation confidence interval.	The model also provides a tool for monitoring individual sites during the testing period. The orange triangles represent values beyond the upper limit of the confidence intervals, the blue triangles represent values below the lower limit and the grey triangles represent values within. 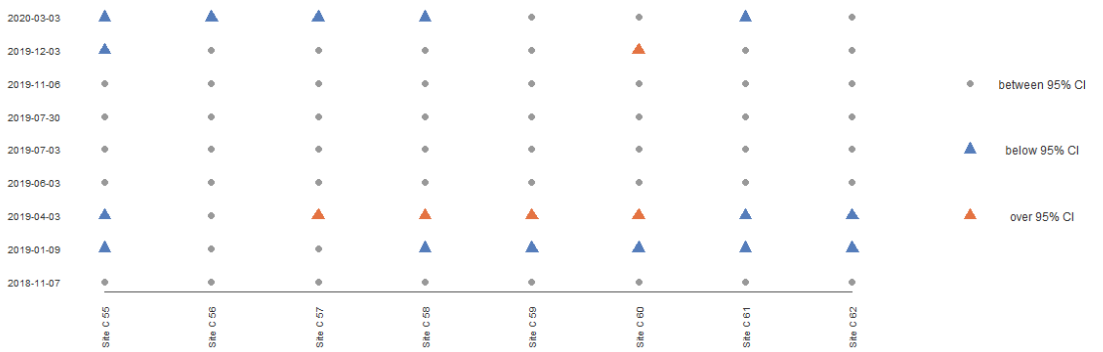
CH_4 (µg/L) (log)	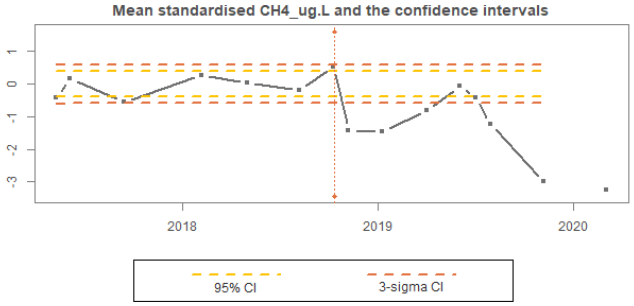 The fitted model has an overall mean of -0.007. The estimated standard deviation of the model residual is 0.183 and the estimated standard deviation of temporal random effect is 0.908. The ratio of random variation over total variation is 0.5. The baseline model provides a measure of the overall performance of all sampling sites. Among the averaged (across sites) standardised data in the testing period, NA out of 9 values fall out of the 95% confidence intervals, and NA fall out of the three times standard deviation confidence interval.	The model also provides a tool for monitoring individual sites during the testing period. The orange triangles represent values beyond the upper limit of the confidence intervals, the blue triangles represent values below the lower limit and the grey triangles represent values within. 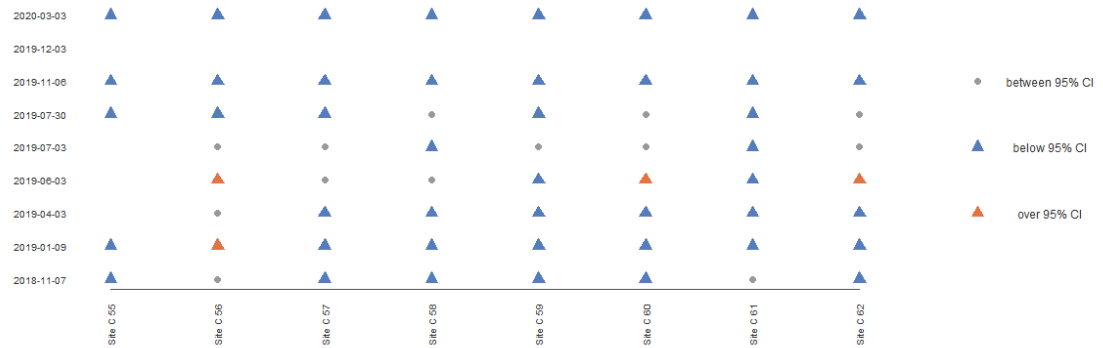

3.4 ORGANIC COMPOUNDS

A comprehensive suite of organic compounds was measured during the phase of monitoring. These included VOCs, SVOCs, phenols, PAHs and phthalates. In addition, acrylamide was measured in some samples as an investigation specifically for evidence of contamination from any hydraulic fracturing fluid since the fluid was reported by the operator to contain polyacrylamide. Table 2 shows the limits of detection (LOD) and numbers of detects for given analytes for individual sites over the period of monitoring. Values were almost invariably below LODs, with the exception of Site 23, which had detectable concentrations of phenol and 4-methylphenol (2 and 5 µg/L respectively) on one sampling occasion (August 2020). Phenol could be derived from organic matter or surface contamination (the site is a private shallow well). None of the analytes determined was detected in any of the PNR boreholes. The data show no evidence of contamination from hydraulic fracturing or other sub-surface activities.

Table 2. Numbers of detections of given organic compounds for given sites determined in Fylde groundwater samples since March 2020; LOD units in µg/L

Analyte	LOD	Site 3	Site 6	Site 7	Site 9	Site 10	Site 21	Site 23	Site 26	Site 54	Site 57	Site 58	Site 62	Site 66
No. samples		4	2	3	3	4	3	4	2	1	2	2	5	1
2-Chlorophenol	<1	0	0	0	0	0	0	0	0	0	0	0	0	0
2-Methylphenol	<0.5	0	0	0	0	0	0	0	0	0	0	0	0	0
2-Nitrophenol	<0.5	0	0	0	0	0	0	0	0	0	0	0	0	0
2,4-Dichlorophenol	<0.5	0	0	0	0	0	0	0	0	0	0	0	0	0
2,4-Dimethylphenol	<1	0	0	0	0	0	0	0	0	0	0	0	0	0
2,4,5-Trichlorophenol	<0.5	0	0	0	0	0	0	0	0	0	0	0	0	0
2,4,6-Trichlorophenol	<1	0	0	0	0	0	0	0	0	0	0	0	0	0
4-Chloro-3-methylphenol	<0.5	0	0	0	0	0	0	0	0	0	0	0	0	0
4-Methylphenol	<1	0	0	0	0	0	0	1	0	0	0	0	0	0
4-Nitrophenol	<10	0	0	0	0	0	0	0	0	0	0	0	0	0
Pentachlorophenol	<1	0	0	0	0	0	0	0	0	0	0	0	0	0
Phenol	<1	0	0	0	0	0	0	1	0	0	0	0	0	0
2-Chloronaphthalene	<1	0	0	0	0	0	0	0	0	0	0	0	0	0
2-Methylnaphthalene	<1	0	0	0	0	0	0	0	0	0	0	0	0	0
Naphthalene	<1	0	0	0	0	0	0	0	0	0	0	0	0	0
Acenaphthylene	<0.5	0	0	0	0	0	0	0	0	0	0	0	0	0
Acenaphthene	<1	0	0	0	0	0	0	0	0	0	0	0	0	0
Fluorene	<0.5	0	0	0	0	0	0	0	0	0	0	0	0	0
Phenanthrene	<0.5	0	0	0	0	0	0	0	0	0	0	0	0	0
Anthracene	<0.5	0	0	0	0	0	0	0	0	0	0	0	0	0
Fluoranthene	<0.5	0	0	0	0	0	0	0	0	0	0	0	0	0
Pyrene	<0.5	0	0	0	0	0	0	0	0	0	0	0	0	0
Benzo(a)anthracene	<0.5	0	0	0	0	0	0	0	0	0	0	0	0	0
Chrysene	<0.5	0	0	0	0	0	0	0	0	0	0	0	0	0
Benzo(bk)fluoranthene	<1	0	0	0	0	0	0	0	0	0	0	0	0	0
Benzo(a)pyrene	<1	0	0	0	0	0	0	0	0	0	0	0	0	0
Indeno(123cd)pyrene	<1	0	0	0	0	0	0	0	0	0	0	0	0	0
Dibenzo(ah)anthracene	<0.5	0	0	0	0	0	0	0	0	0	0	0	0	0
Benzo(ghi)perylene	<0.5	0	0	0	0	0	0	0	0	0	0	0	0	0
Bis(2-ethylhexyl) phthalate	<5	0	0	0	0	0	0	0	0	0	0	0	0	0

Butylbenzyl phthalate	<1	0	0	0	0	0	0	0	0	0	0	0	0	0						
Di-n-butyl phthalate	<1.5	0	0	0	0	0	0	0	0	0	0	0	0	0						
Di-n-Octyl phthalate	<1	0	0	0	0	0	0	0	0	0	0	0	0	0						
Diethyl phthalate	<1	0	0	0	0	0	0	0	0	0	0	0	0	0						
Dimethyl phthalate	<1	0	0	0	0	0	0	0	0	0	0	0	0	0						
1,2-Dichlorobenzene	<1	0	0	0	0	0	0	0	0	0	0	0	0	0						
1,2,4-Trichlorobenzene	<1	0	0	0	0	0	0	0	0	0	0	0	0	0						
1,3-Dichlorobenzene	<1	0	0	0	0	0	0	0	0	0	0	0	0	0						
1,4-Dichlorobenzene	<1	0	0	0	0	0	0	0	0	0	0	0	0	0						
2-Nitroaniline	<1	0	0	0	0	0	0	0	0	0	0	0	0	0						
2,4-Dinitrotoluene	<0.5	0	0	0	0	0	0	0	0	0	0	0	0	0						
2,6-Dinitrotoluene	<1	0	0	0	0	0	0	0	0	0	0	0	0	0						
3-Nitroaniline	<1	0	0	0	0	0	0	0	0	0	0	0	0	0						
4-Bromophenylphenylether	<1	0	0	0	0	0	0	0	0	0	0	0	0	0						
4-Chloroaniline	<1	0	0	0	0	0	0	0	0	0	0	0	0	0						
4-Chlorophenylphenylether	<1	0	0	0	0	0	0	0	0	0	0	0	0	0						
4-Nitroaniline	<0.5	0	0	0	0	0	0	0	0	0	0	0	0	0						
Azobenzene	<0.5	0	0	0	0	0	0	0	0	0	0	0	0	0						
Bis(2-chloroethoxy)methane	<0.5	0	0	0	0	0	0	0	0	0	0	0	0	0						
Bis(2-chloroethyl)ether	<1	0	0	0	0	0	0	0	0	0	0	0	0	0						
Carbazole	<0.5	0	0	0	0	0	0	0	0	0	0	0	0	0						
Dibenzofuran	<0.5	0	0	0	0	0	0	0	0	0	0	0	0	0						
Hexachlorobenzene	<1	0	0	0	0	0	0	0	0	0	0	0	0	0						
Hexachlorobutadiene	<1	0	0	0	0	0	0	0	0	0	0	0	0	0						
Hexachlorocyclopentadiene	<1	0	0	0	0	0	0	0	0	0	0	0	0	0						
Hexachloroethane	<1	0	0	0	0	0	0	0	0	0	0	0	0	0						
Isophorone	<0.5	0	0	0	0	0	0	0	0	0	0	0	0	0						
N-nitrosodi-n-propylamine	<0.5	0	0	0	0	0	0	0	0	0	0	0	0	0						
Nitrobenzene	<1	0	0	0	0	0	0	0	0	0	0	0	0	0						
Acrylamide (n=1)	<0.1	0	0		0	0		0						0						
Analyte	LOD	Site B 40	Site B 41	Site B 42	Site B 43	Site B 44	Site B 45	Site B 46	Site B 47	Site B 48	Site B 49	Site B 50	Site B 51	Site C 57	Site C 58	Site C 59	Site C 60	Site C 61	Site C 62	
No. samples		3	3	3	3	4	4	4	4	4	2	4	4	1	1	1	1	1	1	
2-Chlorophenol	<1	0	0	0	0	0	0	0	0	0	0	0	0	0	0	0	0	0	0	
2-Methylphenol	<0.5	0	0	0	0	0	0	0	0	0	0	0	0	0	0	0	0	0	0	
2-Nitrophenol	<0.5	0	0	0	0	0	0	0	0	0	0	0	0	0	0	0	0	0	0	
2,4-Dichlorophenol	<0.5	0	0	0	0	0	0	0	0	0	0	0	0	0	0	0	0	0	0	
2,4-Dimethylphenol	<1	0	0	0	0	0	0	0	0	0	0	0	0	0	0	0	0	0	0	
2,4,5-Trichlorophenol	<0.5	0	0	0	0	0	0	0	0	0	0	0	0	0	0	0	0	0	0	
2,4,6-Trichlorophenol	<1	0	0	0	0	0	0	0	0	0	0	0	0	0	0	0	0	0	0	
4-Chloro-3-methylphenol	<0.5	0	0	0	0	0	0	0	0	0	0	0	0	0	0	0	0	0	0	
4-Methylphenol	<1	0	0	0	0	0	0	0	0	0	0	0	0	0	0	0	0	0	0	
4-Nitrophenol	<10	0	0	0	0	0	0	0	0	0	0	0	0	0	0	0	0	0	0	
Pentachlorophenol	<1	0	0	0	0	0	0	0	0	0	0	0	0	0	0	0	0	0	0	
Phenol	<1	0	0	0	0	0	0	0	0	0	0	0	0	0	0	0	0	0	0	
2-Chloronaphthalene	<1	0	0	0	0	0	0	0	0	0	0	0	0	0	0	0	0	0	0	
2-Methylnaphthalene	<1	0	0	0	0	0	0	0	0	0	0	0	0	0	0	0	0	0	0	
Naphthalene	<1	0	0	0	0	0	0	0	0	0	0	0	0	0	0	0	0	0	0	
Acenaphthylene	<0.5	0	0	0	0	0	0	0	0	0	0	0	0	0	0	0	0	0	0	
Acenaphthene	<1	0	0	0	0	0	0	0	0	0	0	0	0	0	0	0	0	0	0	
Fluorene	<0.5	0	0	0	0	0	0	0	0	0	0	0	0	0	0	0	0	0	0	
Phenanthrene	<0.5	0	0	0	0	0	0	0	0	0	0	0	0	0	0	0	0	0	0	
Anthracene	<0.5	0	0	0	0	0	0	0	0	0	0	0	0	0	0	0	0	0	0	
Fluoranthene	<0.5	0	0	0	0	0	0	0	0	0	0	0	0	0	0	0	0	0	0	
Pyrene	<0.5	0	0	0	0	0	0	0	0	0	0	0	0	0	0	0	0	0	0	
Benzo(a)anthracene	<0.5	0	0	0	0	0	0	0	0	0	0	0	0	0	0	0	0	0	0	
Chrysene	<0.5	0	0	0	0	0	0	0	0	0	0	0	0	0	0	0	0	0	0	

Benzo(bk)fluoranthene	<1	0	0	0	0	0	0	0	0	0	0	0	0	0	0	0	0	0	0
Benzo(a)pyrene	<1	0	0	0	0	0	0	0	0	0	0	0	0	0	0	0	0	0	0
Indeno(123cd)pyrene	<1	0	0	0	0	0	0	0	0	0	0	0	0	0	0	0	0	0	0
Dibenzo(ah)anthracene	<0.5	0	0	0	0	0	0	0	0	0	0	0	0	0	0	0	0	0	0
Benzo(ghi)perylene	<0.5	0	0	0	0	0	0	0	0	0	0	0	0	0	0	0	0	0	0
Bis(2-ethylhexyl) phthalate	<5	0	0	0	0	0	0	0	0	0	0	0	0	0	0	0	0	0	0
Butylbenzyl phthalate	<1	0	0	0	0	0	0	0	0	0	0	0	0	0	0	0	0	0	0
Di-n-butyl phthalate	<1.5	0	0	0	0	0	0	0	0	0	0	0	0	0	0	0	0	0	0
Di-n-Octyl phthalate	<1	0	0	0	0	0	0	0	0	0	0	0	0	0	0	0	0	0	0
Diethyl phthalate	<1	0	0	0	0	0	0	0	0	0	0	0	0	0	0	0	0	0	0
Dimethyl phthalate	<1	0	0	0	0	0	0	0	0	0	0	0	0	0	0	0	0	0	0
1,2-Dichlorobenzene	<1	0	0	0	0	0	0	0	0	0	0	0	0	0	0	0	0	0	0
1,2,4-Trichlorobenzene	<1	0	0	0	0	0	0	0	0	0	0	0	0	0	0	0	0	0	0
1,3-Dichlorobenzene	<1	0	0	0	0	0	0	0	0	0	0	0	0	0	0	0	0	0	0
1,4-Dichlorobenzene	<1	0	0	0	0	0	0	0	0	0	0	0	0	0	0	0	0	0	0
2-Nitroaniline	<1	0	0	0	0	0	0	0	0	0	0	0	0	0	0	0	0	0	0
2,4-Dinitrotoluene	<0.5	0	0	0	0	0	0	0	0	0	0	0	0	0	0	0	0	0	0
2,6-Dinitrotoluene	<1	0	0	0	0	0	0	0	0	0	0	0	0	0	0	0	0	0	0
3-Nitroaniline	<1	0	0	0	0	0	0	0	0	0	0	0	0	0	0	0	0	0	0
4-Bromophenylphenylether	<1	0	0	0	0	0	0	0	0	0	0	0	0	0	0	0	0	0	0
4-Chloroaniline	<1	0	0	0	0	0	0	0	0	0	0	0	0	0	0	0	0	0	0
4-Chlorophenylphenylether	<1	0	0	0	0	0	0	0	0	0	0	0	0	0	0	0	0	0	0
4-Nitroaniline	<0.5	0	0	0	0	0	0	0	0	0	0	0	0	0	0	0	0	0	0
Azobenzene	<0.5	0	0	0	0	0	0	0	0	0	0	0	0	0	0	0	0	0	0
Bis(2-chloroethoxy)methane	<0.5	0	0	0	0	0	0	0	0	0	0	0	0	0	0	0	0	0	0
Bis(2-chloroethyl)ether	<1	0	0	0	0	0	0	0	0	0	0	0	0	0	0	0	0	0	0
Carbazole	<0.5	0	0	0	0	0	0	0	0	0	0	0	0	0	0	0	0	0	0
Dibenzofuran	<0.5	0	0	0	0	0	0	0	0	0	0	0	0	0	0	0	0	0	0
Hexachlorobenzene	<1	0	0	0	0	0	0	0	0	0	0	0	0	0	0	0	0	0	0
Hexachlorobutadiene	<1	0	0	0	0	0	0	0	0	0	0	0	0	0	0	0	0	0	0
Hexachlorocyclopentadiene	<1	0	0	0	0	0	0	0	0	0	0	0	0	0	0	0	0	0	0
Hexachloroethane	<1	0	0	0	0	0	0	0	0	0	0	0	0	0	0	0	0	0	0
Isophorone	<0.5	0	0	0	0	0	0	0	0	0	0	0	0	0	0	0	0	0	0
N-nitrosodi-n-propylamine	<0.5	0	0	0	0	0	0	0	0	0	0	0	0	0	0	0	0	0	0
Nitrobenzene	<1	0	0	0	0	0	0	0	0	0	0	0	0	0	0	0	0	0	0
Acrylamide (n=1)	<0.05	0	0	0	0	0	0	0	0	0	0	0	0	0	0	0	0	0	0

n: number of analyses; LOD: limit of detection

3.5 REAL-TIME MONITORING

Real-time monitoring of groundwater from boreholes in the Fylde continued during the phase of investigation. Data for specific electrical conductance (SEC) are shown in Figure 13. SEC values are prone to variation with calibration, uncertainties in which result in small step changes in observations; vertical lines indicate where sondes have been removed from boreholes for recalibration on site. Sensor EBM5 also has a relatively spiky trend during 2020–2021, possibly an artefact of sensor instability rather than real variation in groundwater quality (salinity). However, the traces show the long-term trend in SEC for the site and the sensor location is within the PNR borehole cluster so the data have been retained in the plot. There appears little evidence for major changes in salinity of groundwater post-hydraulic fracturing.

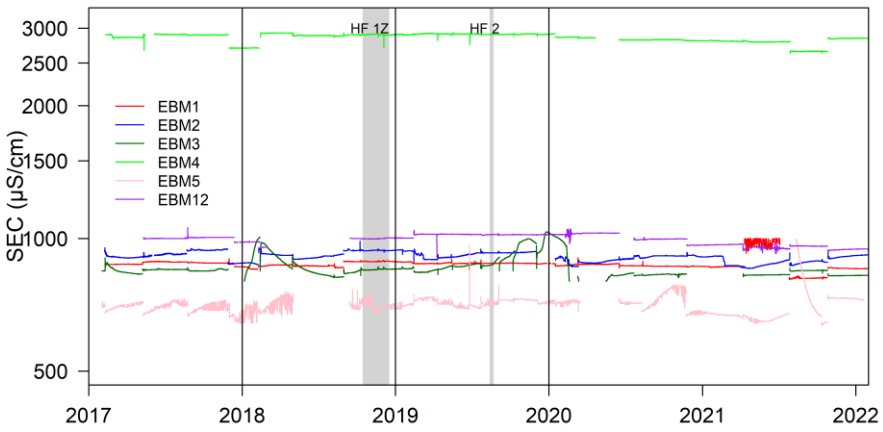

Figure 13. Real-time monitoring data for specific electrical conductance (SEC) in sensors installed in the Fylde; EBM1, 5 and 12 are located in the Preston New Road borehole cluster; periods of hydraulic fracturing of PNR borehole 1Z and 2 shown by grey bars

4 Concluding remarks

The Phase 6 project has involved monitoring of GHGs at PNR and water quality in the Quaternary aquifer and streams around PNR for the years 2020 and 2021 and represents the final phase of monitoring in the Fylde in connection with unconventional hydrocarbon exploration.

The report concludes the monitoring of GHGs at PNR after five years of measurements. GHGs were measured for two years prior to hydraulic fracturing, for roughly two years, during which operational exploratory activity took place, and for roughly a year after the closure of the facility. We diagnosed and quantified a single, episodic emission event which was conclusively associated with flowback operations. This event involved the direct venting of 4.2 tonnes of methane to atmosphere, in breach of operational permit (see Shaw et al., 2020 for details). No other transient GHG emissions associated with hydraulic fracturing operations were conclusively identified over the course of monitoring.

The programme has facilitated the development of measurement and data-quality protocols for continuous monitoring of industrial pollution sources using high-precision instrumentation. The programme has also equipped UK academic and regulatory bodies with tools and approaches for conducting rigorous baseline and climatological analyses prior to the onset of industrial activity. Such an approach allows for enhanced certainty in detecting and quantifying the impacts of new industrial activity on local atmospheric composition. We have demonstrated the importance of optimising the monitoring station location by taking advantage of local wind conditions and the prevalence of cleaner air under westerly winds at PNR. Optimal positioning of the monitoring site generally requires a location downwind of sources of interest in a direction that minimises the potential for interference from extraneous sources. This is quite often to the east of sources in the UK (benefitting from cleaner Atlantic maritime background air masses) but a localised assessment will always be necessary to determine this. A year of baseline measurements is the recommended minimum for capturing seasonal cycles in pollutant concentrations (Shaw et al., 2019). A statistical GHG climatology should ideally consist of (as a minimum) mean average, standard deviation, and quartile and decile statistics quantified as a function of wind direction for each pollutant. Such data were demonstrated to underpin emission identification from the PNR facility by Shaw et al. (2020). However, robust emission detection,

and attribution of those emissions, remains challenging and is dependent on multiple factors including; the magnitude of the emission event(s), the location and size of other emission sources, and local meteorology. Emission detection and attribution can be greatly aided by a comprehensive comparative baseline, the measurement of any potential co-emitted pollutants, and the derivation of statistical climatologies. Nascent work indicates that machine-learning approaches may offer much promise to automated emission detection, however this remains an academic endeavour at present. A statistical climatological method, analogous to that described in Shaw et al. (2020), is recommended here and has been demonstrated to be fit for purpose in annual reports and academic papers, and could (in the authors' opinions) be recommended to policy makers when planning for and carrying out monitoring in the future.

The report also concludes monitoring of groundwater and surface-water quality after up to six years of measurements in the Fylde. The data have demonstrated the large spatial and temporal variability in water quality and the large complexities of establishing baseline conditions and detecting change. The water-quality dataset has been investigated using a statistical model. This greatly simplifies the observed variations in concentrations of a selected number of analytes. Given the large heterogeneity in chemical compositions over space and time and the limitations of spatial and temporal coverage of data, it is not possible to produce a model that encompasses the full complexity of chemical variation. The simplified model has limitations in carrying a potential to miss real changes or alternatively highlight compositions as inconsistent with baseline (outside the confidence intervals). Nonetheless, the model provides an approach for investigating changes which can prompt further more detailed investigation. Moreover, the statistical approach used should be applicable more widely for addressing change detection in water-monitoring programmes.

Should hydraulic fracturing for shale-gas extraction restart in the UK in the future, either at the sites studied as part of this programme or elsewhere, we recommend that atmospheric composition monitoring facilities analogous to those used in this programme be reinstalled to continue accurate high-quality monitoring to inform regulation and public stakeholders. Where possible, monitoring stations should be placed downwind in the local prevailing wind direction so as to increase the likelihood of sampling industrial emissions should they occur. Monitoring should also be commissioned to take place before industrial activity to conduct baseline and climatological analyses, and should continue throughout and beyond the lifetime of the proposed industry to monitor and quantify both concurrent emissions and legacy emissions. In summary, this work has been highly specific to the exploratory hydraulic fracturing facilities studied and data cannot easily be extrapolated to any future activity. The recommendation for future monitoring, under baseline and post-baseline conditions, applies equally to groundwater and surface-water quality, as there remains a strong public interest and questions concerning environmental impacts of sub-surface exploration.

5 References

Allen, G., Shaw, J., Shah, A., Pitt, J., Ricketts, H., Williams, P. and Ward, R.: Environmental baseline monitoring project: Methane enhancements detected at Little Plumpton air monitoring site, Nottingham, UK, British Geological Survey, https://www.bgs.ac.uk/news/item.cfm?id=9410, 2019.

Boothroyd, I. M., Almond, S., Qassim, S. M., Worrall, F. and Davies, R. J.: Fugitive emissions of methane from abandoned, decommissioned oil and gas wells, Sci. Tot. Env., 547, 461-469, https://doi.org/10.1016/j.scitotenv.2015.12.096, 2016.

Environment Agency. 2019. EPR Compliance Assessment Report. Preston New Road Exploration Site EPR/AB3101MW. Report ID: UP3431VF/0348127, Environment Agency.

Environment Agency. 2020. EPR Compliance Assessment Report. Preston New Road Exploration Site EPR/AB3101MW. Report ID: UP3431VF/0358308, Environment Agency.

Grange, S. K., Carslaw, D. C., Lewis, A. C., Boleti, E. and Hueglin, C.: Random forest meteorological normalisation models for Swiss PM_{10} trend analysis, Atmos. Chem. Phys., 18, 6223-6239, https://doi.org/10.5194/acp-18-6223-2018, 2018.

Grange, S. K. and Carslaw, D. C.: Using meteorological normalisation to detect interventions in air quality time series, Sci. Tot. Env., 653, 578-588, https://doi.org/10.1016/j.scitotenv.2018.10.344, 2019.

Grange, S. K., Lee, J. D., Drysdale, W. S., Lewis, A. C., Hueglin, C., Emmenegger, L., Carslaw, D. C.: COVID-19 lockdowns highlight a risk of increasing ozone pollution in European urban areas, Atmos. Chem. Phys., 21, 4169-4185, https://doi.org/10.5194/acp-21-4169-2021, 2021.

Lan, X., Nisbet, E. G., Dlugokencky, E. J. and Michel, S. E.: What do we know about the global methane budget? Results from four decades of atmospheric CH_4 observations and the way forward, Phil. Trans. R. Soc. A., 379, https://doi.org/10.1098/rsta.2020.0440, 2021.

Lovrić, M., Pavlović, K., Vuković, M., Grange, S. K., Haberl, M. and Kern, R.: Understanding the true effects of the COVID-19 lockdown on air pollution by means of machine learning, Environ. Pollut., 274, 115900, https://doi.org/10.1016/j.envpol.2020.115900, 2021.

Lowry, D. L., Fisher, R. E., France, J. L., Coleman, M., Lanoisellé, M., Zazzeri, G., Nisbet, E. G., Shaw, J. T., Allen, G., Pitt, J. and Ward, R. S.: Environmental baseline monitoring for shale gas development in the UK: Identification and geochemical characterisation of local source emissions of methane to atmosphere, Sci. Tot. Env., 708, 134600, https://doi.org/10.1016/j.scitotenv.2019.134600, 2020.

Purvis, R. M., Lewis, A. C., Hopkins, J. R., Wilde, S. E., Dunmore, R. E., Allen, G., Pitt, J. and Ward, R. S.: Effects of 'pre-fracking' operations on ambient air quality at a shale gas exploration site in rural North Yorkshire, England, Sci. Tot. Env., 673, 445-454, https://doi.org/10.1016/j.scitotenv.2019.04.077, 2019.

Riddick, S. N., Mauzerall, D. L., Celia, M. A., Kang, M. and Bandilla, K.: Variability observed over time in methane emissions from abandoned oil and gas wells, Int. J. Greenhouse Gas Control, 100, 103116, https://doi.org/10.1016/j.ijggc.2020.103116, 2020.

Sandl, E., Cahill, A. G., Welch, L. and Beckie, R.: Characterizing oil and gas wells with fugitive gas migration though Bayesian multilevel logistic regression, Sci. Tot. Env., 769, 144678, https://doi.org/10.1016/j.scitotenv.2020.144678, 2021.

Shah, A., Ricketts, H., Pitt, J. R., Shaw, J. T., Kabbabe, K., Leen, J. B., Allen, G.: Unmanned aerial vehicle observations of cold venting from exploratory hydraulic fracturing in the United Kingdom, Env. Res. Comm., 2, 021003, https://doi.org/10.1088/2515-7620/ab716d, 2020a.

Shah, A., Pitt, J. R., Ricketts, H., Leen, J. B., Williams, P. I., Kabbabe, K., Gallagher, M. W. and Allen, G.: Testing the near-field Gaussian plume inversion flux quantification technique using unmanned aerial vehicle sampling, Atmos. Meas. Tech., 13, 1467-1484, https://doi.org/10.5194/amt-13-1467-2020, 2020b.

Shaw, J. T., Allen, G., Pitt, J., Mead, M. I., Purvis, R. M., Dunmore, R., Wilde, S., Shah, A., Barker, P., Bateson, P., Bacak, A., Lewis, A. C., Lowry, D., Fisher, R., Lanoisellé, M. and Ward, R. S.: A baseline of atmospheric greenhouse gases for prospective UK shale gas sites, Sci. Tot. Env., 684, 1-13, https://doi.org/10.1016/j.scitotenv.2019.05.266, 2019.

Shaw, J. T., Allen, G., Pitt, J., Shah, A., Wilde, S., Stamford, L., Fan, Z., Ricketts, H., Williams, P. I., Bateson, P., Barker, P., Purvis, R., Lowry, D., Fisher, R., France, J., Coleman, M., Lewis, A. C., Risk, D. A. and Ward, R. S.: Methane flux from flowback operations at a shale gas site, JAPCA J. Air Waste Ma., 70, https://doi.org/10.1080/10962247.2020.1811800, 2020.

Shi, Z., Song, C., Liu, B., Lu, G., Xu, J., Vu, T. V., Elliott, R. J. R., Li, W., Bloss, W. J. and Harrison, R. M.: Abrupt but smaller than expected changes in surface air quality attributable to COVID-19 lockdowns, Science Advances, 7, 3, https://doi.org/10.1126/sciadv.abd6696, 2021.

Taylor, S. J. and Letham, B.: Forecasting at scale, Am. Stat., 72, 37-45, https://doi.org/10.1080/00031305.2017.1380080, 2018.

Topping, D., Watts, D., Coe, H., Evans, J., Bannan, T. J., Lowe, D., Jay, C. and Taylor, J. W.: Evaluating the use of Facebook's Prophet model v0.6 in forecasting concentration of NO_2 at single sites across the UK and in response to the COVID-19 lockdown in Manchester, England, Geosci. Model Dev., In review, https://doi.org/10.5194/gmd-2020-270, 2020.

Ward, R.S., Allen, G., Baptie, B.J., Bateson, L., Bell, R.A., Butcher, A.S., Daraktchieva, Z., Dunmore, R., Fisher, R.E., Horleston, A., Howarth, C.H., Jones, D.G., Jordan, C.J., Kendall, M., Lewis, A., Lowry, D., Miller, C.A., Milne, C.J., Novellino, A., Pitt, J., Purvis, R.M., Smedley, P.L., Wasikiewicz, J.M. Preliminary assessment of the environmental baseline in the Fylde, Lancashire. British Geological Survey Open Report OR/18/020, Keyworth, UK, 104 pp. 2018a.

Ward, R. S., Smedley, P. L., Allen, G., Baptie, B. J., Daraktchieva, Z., Horleston, A., Jones, D. G., Jordan, C. J., Lewis, A., Lowry, D., Purvis, R. M. and Rivett, M. O.: Environmental Baseline Monitoring Project: Phase II Final Report. British Geological Survey Open Report OR/17/049, Keyworth, UK, 2017.

Ward, R. S., Smedley, P. L., Allen, G., Baptie, B. J., Cave, M. R., Daraktchieva, Z., Fisher, R., Hawthorn, D., Jones, D. G., Lewis, A., Lowry, D., Luckett, R., Marchant, B. P., Purvis, R. M. and Wilde, S.: Environmental Baseline Monitoring: Phase III Final Report (2017–2018). British Geological Survey Open Report OR/18/026, Keyworth, UK, 2018b.

Ward, R. S., Smedley, P. L., Allen, G., Baptie, B. J., Barkwith, A. K. A. P., Bateson, L., Bell, R. A., Bowes, M., Coleman, M., Cremen, G., Daraktchieva, Z., Gong, M., Howarth, C. H., Fisher, R., Hawthorn, D., Jones, D. G., Jordan, C., Lanoiselle, M., Lewis, A. C., Lister, T. R., Lowry, D., Luckett, R., Mallin-Martin, D., Marchant, B. P., Miller, C. A., Milne, C. J., Novellino, A., Pitt, J., Purvis, R. M., Rivett, M. O., Shaw, J., Taylor-Curran, H., Wasikiewicz, J. M., Werner, M. and Wilde, S.: Environmental Monitoring: Phase 4 Final Report (April 2018–March 2019). British Geological Survey Open Report OR/19/044, Keyworth, UK, 2019.

Ward, R. S., Smedley, P. L., Allen, G., Baptie, B. J., Barker, P., Barwith, A. K. A. P., Bates, P., Bateson, L., Bell, R. A., Coleman, M., Cremen, G., Crewdson, E., Daraktchieva, Z., Gong, M., Howarth, C. H., France, J., Lewis, A. C., Lister, T. R., Lowry, D., Luckett, R., Mallin Martin, D., Marchant, B. P., Miller, C. A., Milne, C. J., Novellino, A., Pitt, J., Purvis, R. M., Rivett, M. O.,

Shaw, J., Taylor-Curran, H., Wasiekiewicz, J. M., Werner, M. and Wilde, S.: Environmental Monitoring: Phase 5 Final Report (April 2019–March 2020). British Geological Survey Open Report OR/20/035, Keyworth, UK, 2020.

Williams, J. P., Regehr, A. and Kang, M.: Methane emissions from abandoned oil and gas wells in Canada and the United States, Environ. Sci. Technol., 55, 1, 563 – 570, https://doi.org/10.1021/acs.est.0c04265, 2021.

Appendix 1 Atmospheric composition of earlier phases

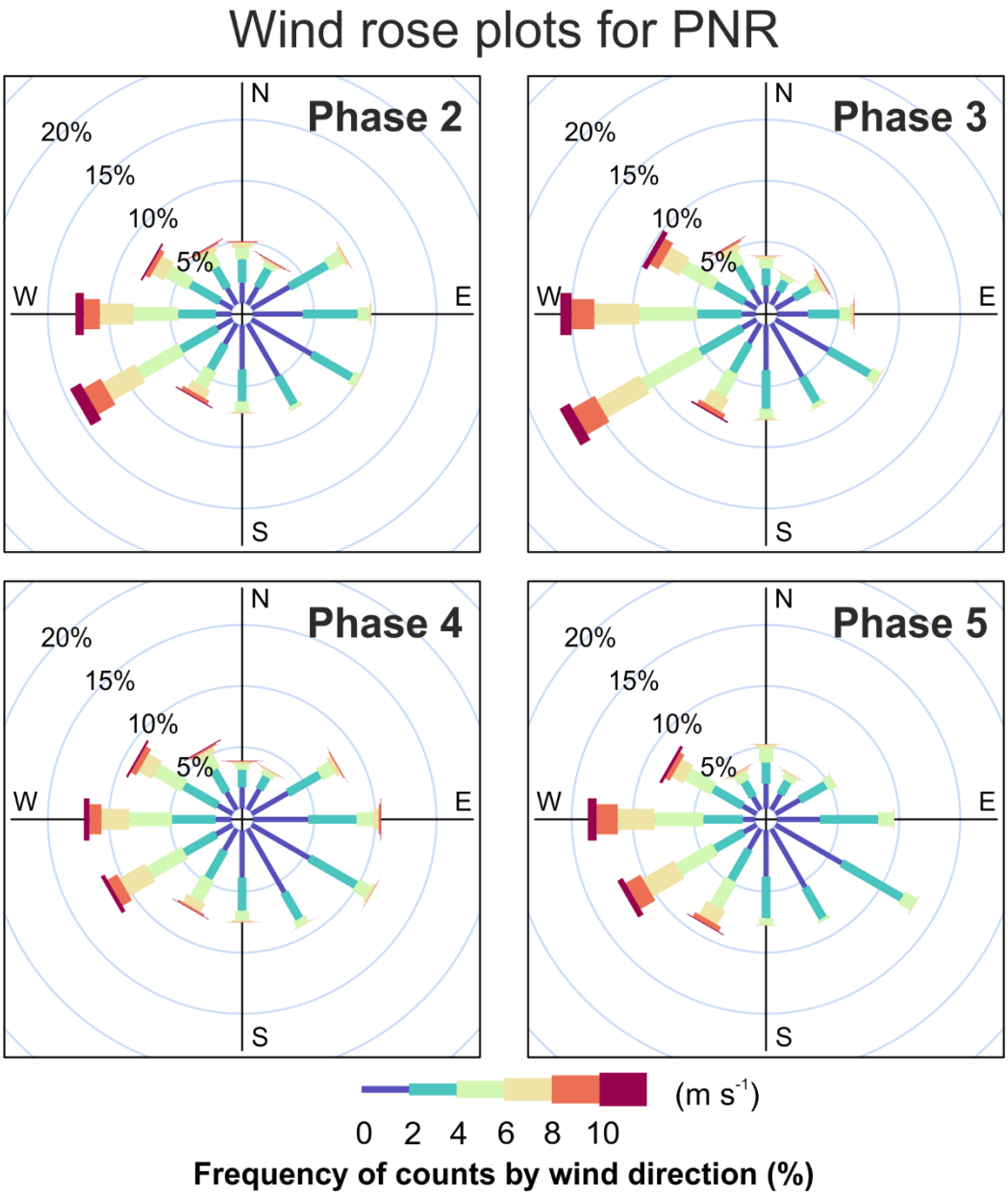

Figure A1. Wind-rose plots for the PNR site showing wind speed and wind direction statistics for Phases 2 through 5. The radii of the paddles show the percentage of total sampling time in each of the 12 30° wind direction cones. The colour and length of the sectors indicate the percentage of time in each wind speed band (see colour legend). © University of Manchester, 2022

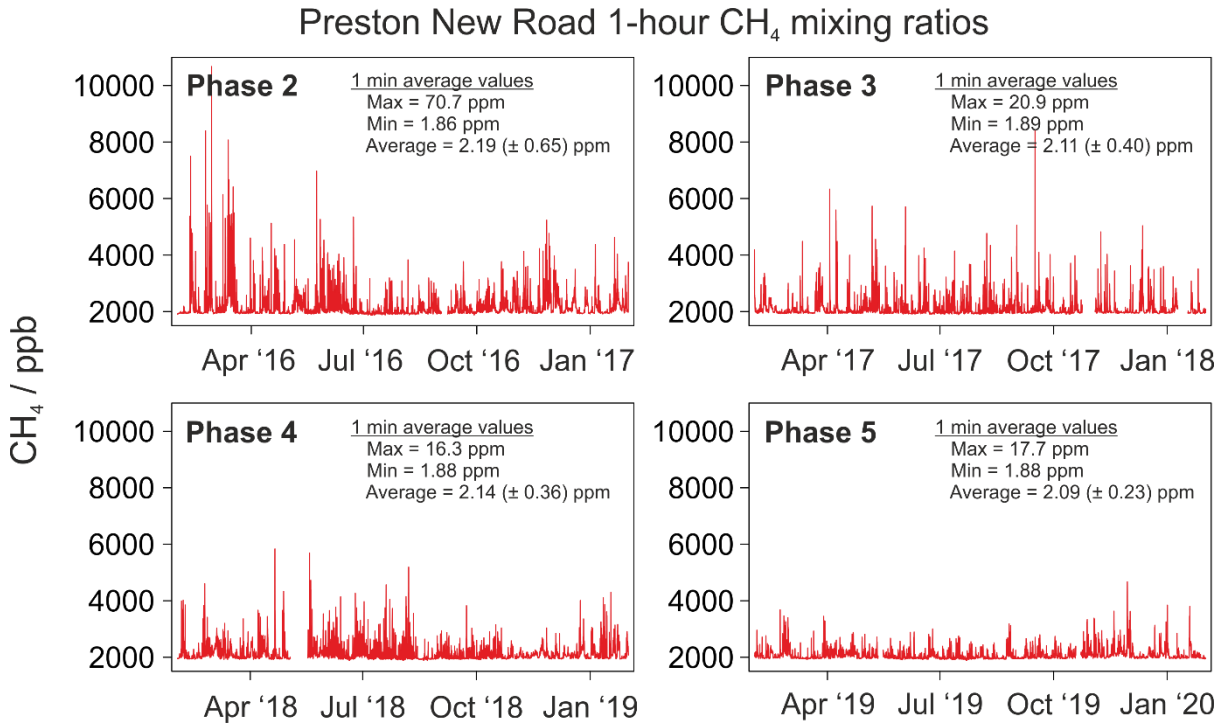

Figure A2. Time-series of one-hour averaged CH_4 mixing ratios measured at PNR during Phases 2 through 5. © University of Manchester, 2022

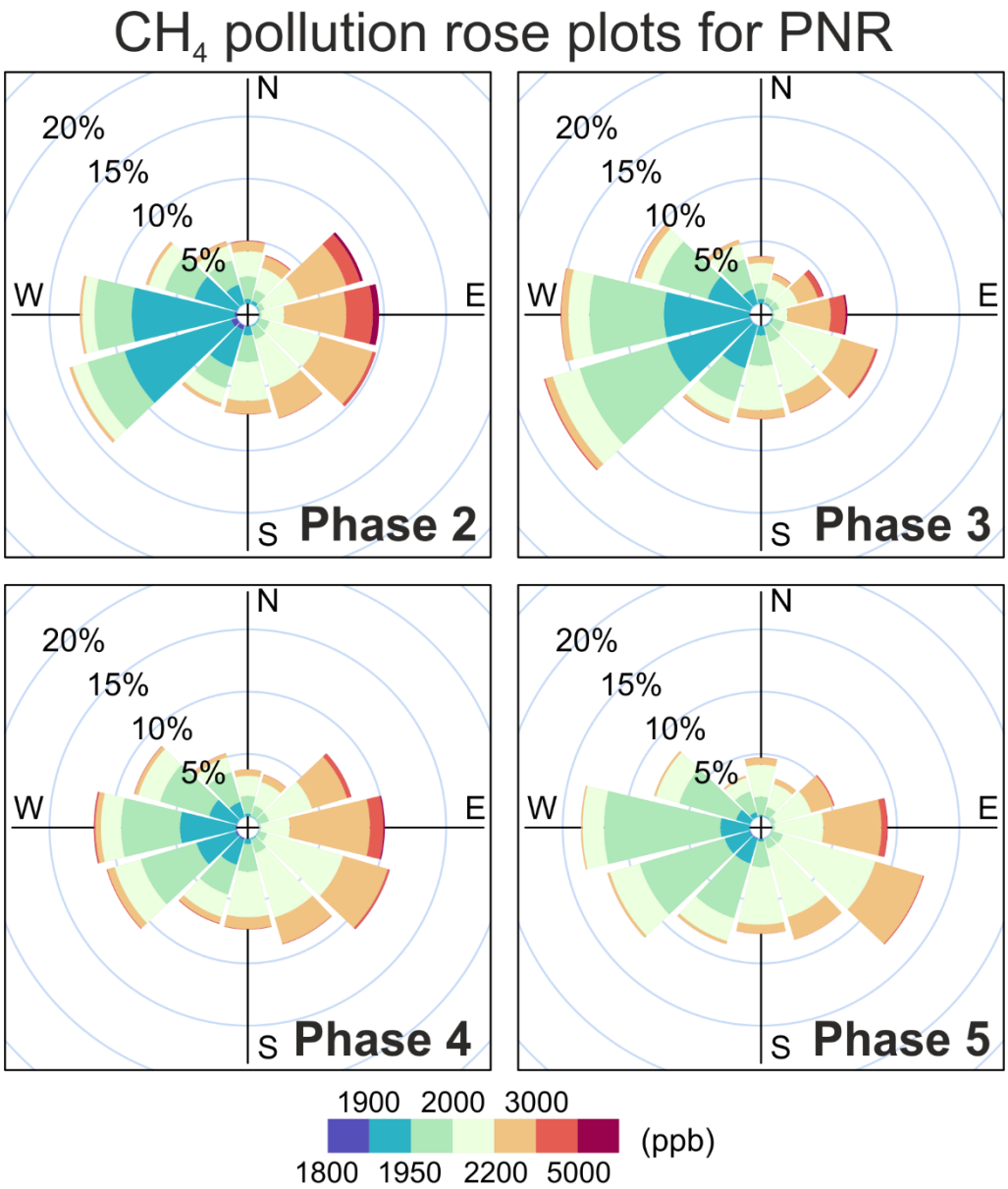

Figure A3. CH_4 concentration-frequency and wind-rose plots showing CH_4 mixing ratios as a function of wind direction during Phases 2 through 5. The radii of the paddles show the percentage of total time in each of the 12 wind direction cones (30° increments relative to true North) and the colour of the paddles show the CH_4 mixing ratio (see colour legend). © University of Manchester, 2022

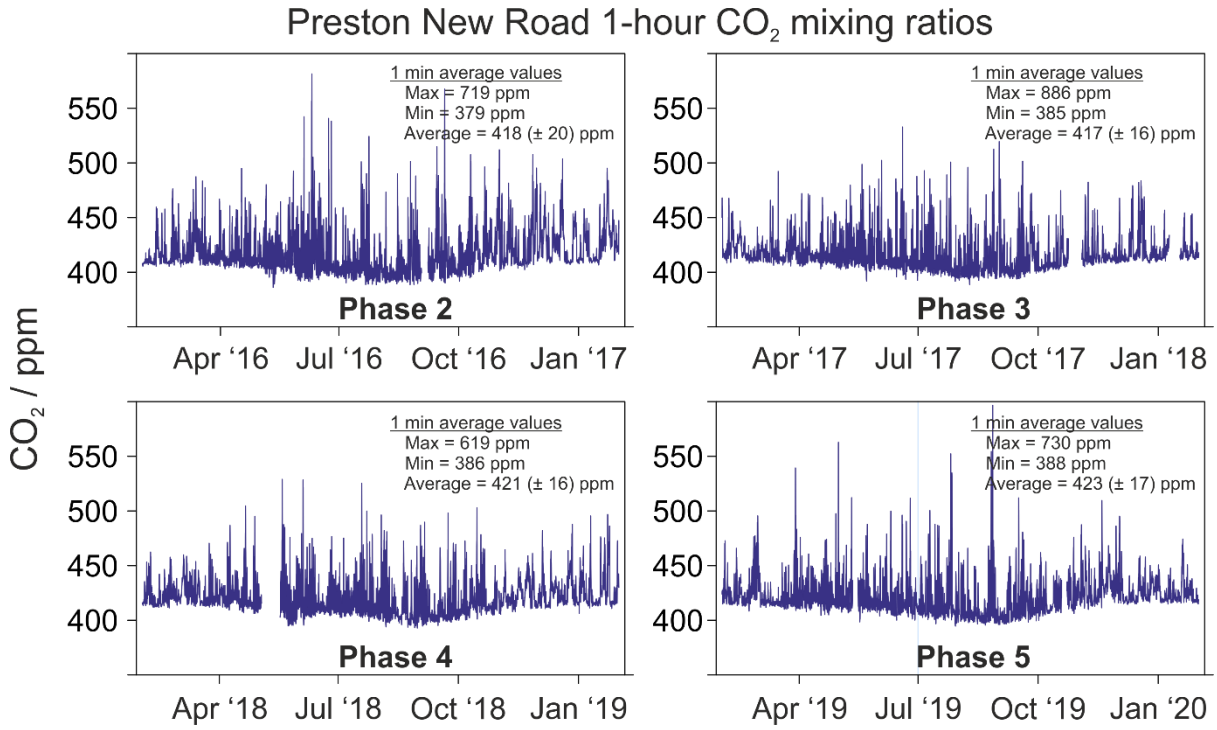

Figure A4. Time series of one-hour averaged CO_2 mixing ratios measured at PNR during Phases 2 through 5. © University of Manchester, 2022

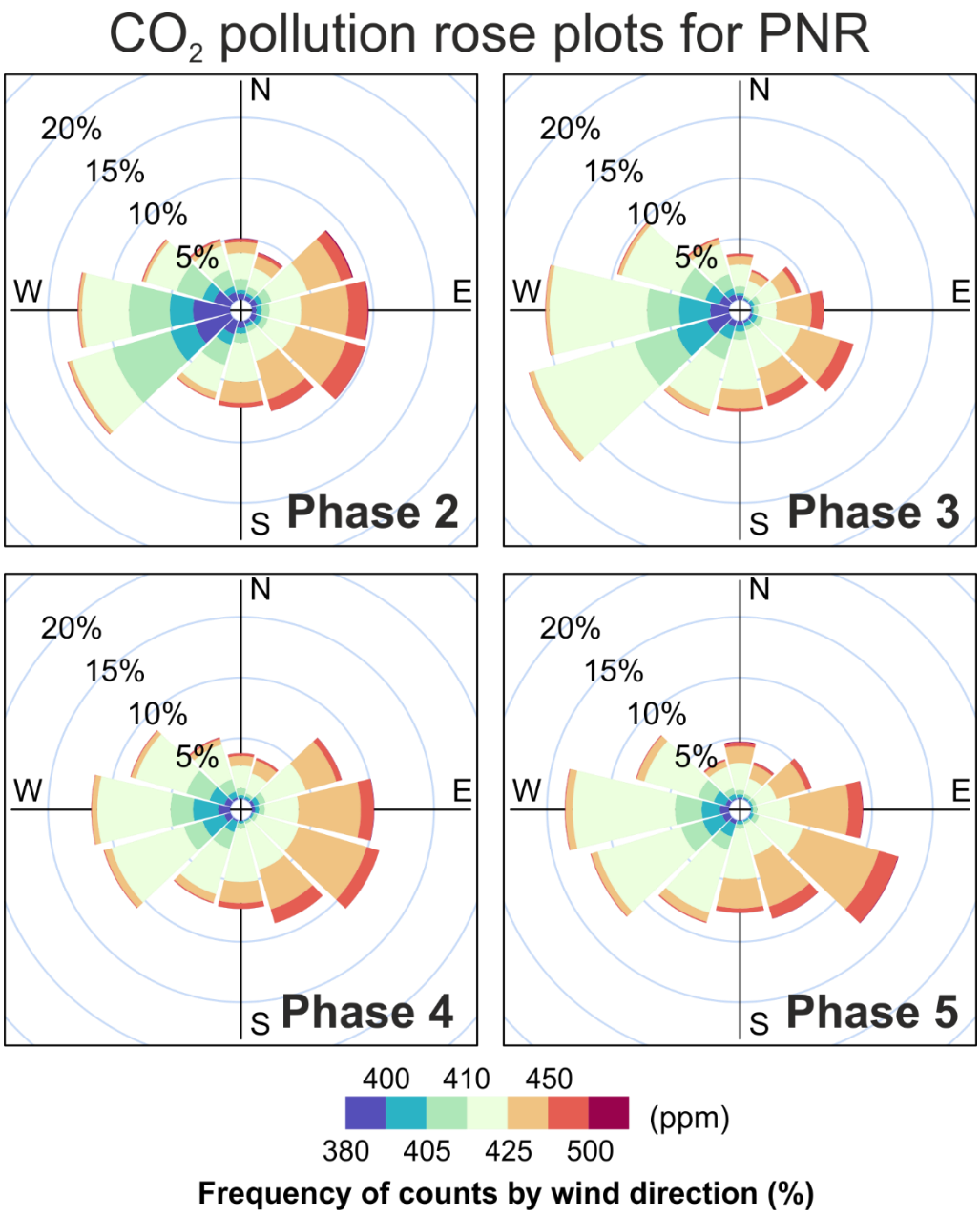

Figure A5. CO_2 concentration-frequency and wind-rose plots showing CO_2 mixing ratios as a function of wind direction during Phases 2 through 5. The radii of the paddles show the percentage of total time in each of the 12 wind direction cones (30° increments relative to true North) and the colour of the paddles show the CO_2 mixing ratio (see colour legend).

Appendix 2 Threshold algorithm for methane emission

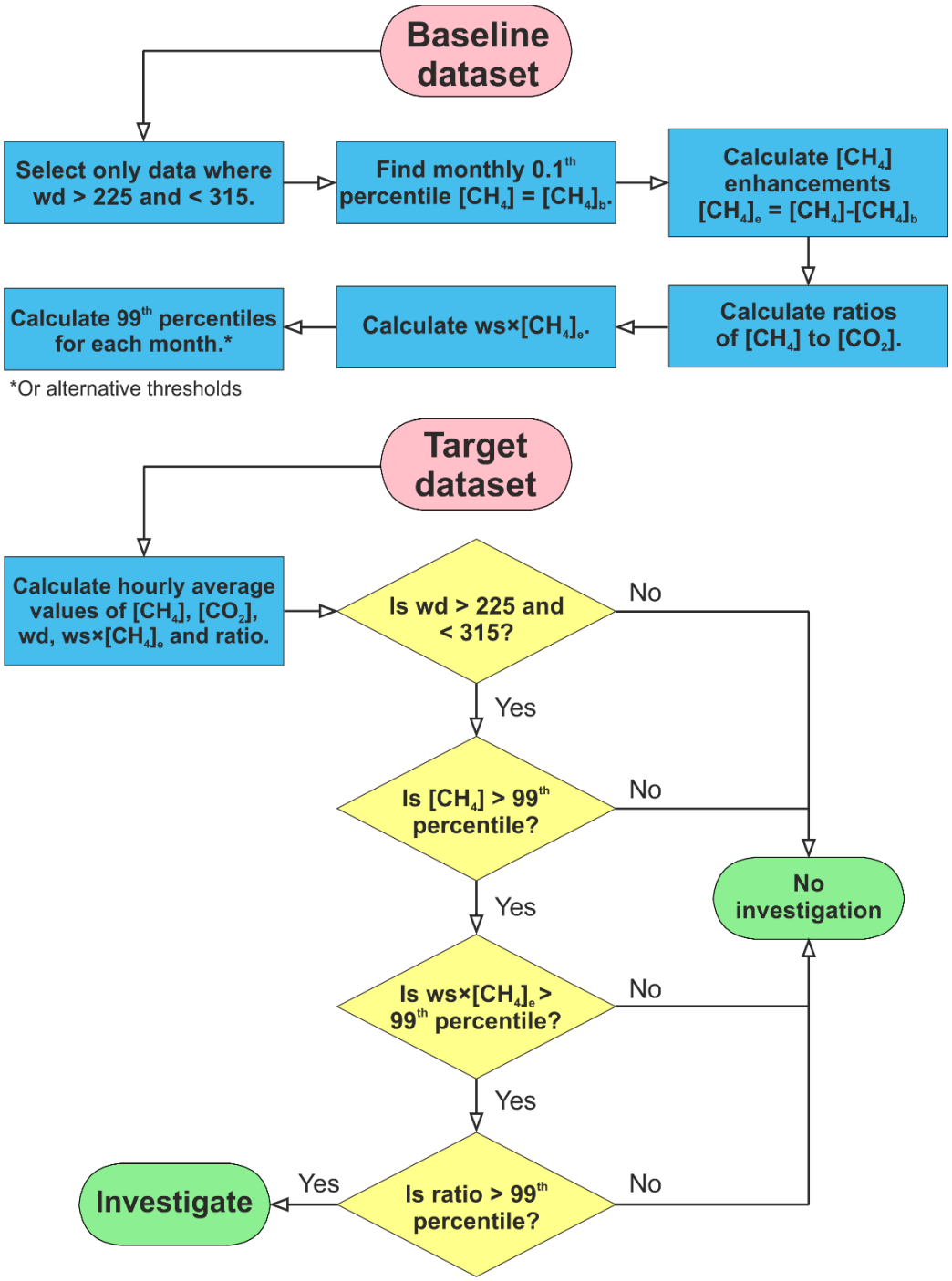

Figure A6. Algorithm for detecting baseline excursion events. Key to abbreviations: $[CH_4]_b$ = 0.1th percentile $[CH_4]$; $[CH_4]_e$ = $[CH_4]$ enhancement = $[CH_4] – [CH_4]_b$; wd = wind direction; ws = wind speed. Wind directions between 225° and 315° incorporate all winds that can be considered to be westerly (i.e. 270° ± 45°).